

Optimizing Orthogonalized Tensor Deflation via Random Tensor Theory

Mohamed El Amine Seddik¹ Mohammed Mahfoud¹ Merouane Debbah¹

Abstract

This paper tackles the problem of recovering a low-rank signal tensor with possibly correlated components from a random noisy tensor, or so-called *spiked tensor model*. When the underlying components are orthogonal, they can be recovered efficiently using *tensor deflation* which consists in successive rank-one approximations, while non-orthogonal components may alter the tensor deflation mechanism, thereby preventing efficient recovery. Relying on recently developed random tensor tools, this paper deals precisely with the non-orthogonal case by deriving an asymptotic analysis of a *parameterized* deflation procedure performed on an order-three and rank-two spiked tensor. Based on this analysis, an efficient tensor deflation algorithm is proposed by optimizing the parameter introduced in the deflation mechanism, which in turn is proven to be optimal by construction for the studied tensor model. The same ideas could be extended to more general low-rank tensor models, e.g., higher ranks and orders, leading to more efficient tensor methods with broader impact on machine learning and beyond.

1. Introduction

Tensor methods have been proven to be a powerful and versatile tool in machine learning in both providing a rich framework for theoretical analysis and motivating the reformulation of existing problems in higher dimensions (Rabanser et al., 2017; Sidiropoulos et al., 2017), which often results in the ability to develop better performing algorithms or massively accelerate existing ones (Fawzi et al., 2022). One of the most fundamental problems in machine learning is retrieving low-rank structures from high-dimensional data, in which tensor methods are particularly successful, e.g., learning Gaussian mixtures in an unsupervised setting (Anandkumar et al., 2014), which can be seen as a natural generalization of the standard principal component analysis (PCA) to higher order tensors (Zare et al., 2018). Another surprising area where tensors methods have been shown to be efficient, is the reconstruction of training samples from a single gradient query of a neural network in a federated learning context (Wang et al., 2022).

As a first step towards understanding the behavior of tensor methods, Richard & Montanari (2014) introduced the concept of tensor PCA by studying the so-called *spiked tensor model* of the form $\beta x^{\otimes d} + \mathcal{W}/\sqrt{p}$ where $x \in \mathbb{R}^p$ is a high-dimensional vector of unit norm which represents the (rank-one) signal of interest, \mathcal{W} is a symmetric Gaussian random noise tensor of order d , and $\beta \geq 0$ is a parameter controlling the signal strength. This statistical model raises many fundamental questions which mainly concern the theoretical and algorithmic guarantees that ensure the efficient recovery of the hidden signal x .

A flurry of works focused on addressing these questions (Perry et al., 2020; Lesieur et al., 2017; Jagannath et al., 2020; Chen et al., 2021; Goulart et al., 2021; Auddy & Yuan, 2022; Ben Arous et al., 2021). The first main result was for tensors of order $d \geq 3$, for which it was shown that there exists a statistical threshold β_{stat} of $O(1)$ in the tensor dimension, which defines the information-theoretic limit above which signal recovery is possible, with the maximum likelihood estimator (MLE), and below which signal recovery is impossible.

While recovery above β_{stat} is theoretically possible from an information-theoretic standpoint, solving the underlying MLE problem remains NP-hard in the worst case (Hillar & Lim, 2013). Indeed, Richard & Montanari (2014) suggests through heuristics that there exists an algorithmic threshold $\beta_{algo} = O(p^{\frac{d-2}{4}})$ beyond which recovery is possible with

¹Technology Innovation Institute, Abu Dhabi, United Arab Emirates. Correspondence to: M. Seddik <mohamed.seddik@tii.ae>, M. Mahfoud <mohammed.mahfoud@tii.ae>, M. Debbah <merouane.debbah@tii.ae>.

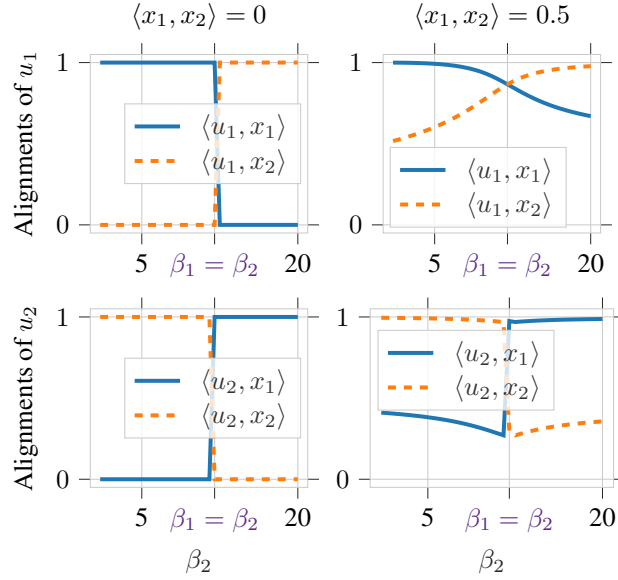


Figure 1. Orthogonalized deflation (see §3.2 for details) applied on the rank-two tensor $\sum_{i=1}^2 \beta_i x_i^{\otimes 3}$ which yields the signal estimates u_1 and u_2 , at first and second deflation steps respectively. The signals are successfully recovered in the orthogonal case $\langle x_1, x_2 \rangle = 0$ (left), while the estimation is altered if the signal components are correlated $\langle x_1, x_2 \rangle = 0.5$ (right). β_1 is fixed while varying β_2 .

a polynomial time algorithm, therefore implying the existence of a theoretical-algorithmic spectral gap where no polynomial time algorithm has been proven to be efficient in signal recovery. These suggestions were rigorously proven by (Lesieur et al., 2017; Jagannath et al., 2020; Chen et al., 2021; Huang et al., 2022) and generalized to non-symmetric tensors by (Ben Arous et al., 2021; Seddik et al., 2021; Audy & Yuan, 2022).

From a practical standpoint, to be able to unleash the full potential of tensor methods, higher (beyond rank-one) low-rank signal reconstruction problems need to be considered, thus motivating the study of *low-rank spiked tensor models*. In particular, and in a more realistic scenario, one would be interested in extracting low-rank hidden structures from random noise, for which the model can naturally be extended to $\sum_{i=1}^r \beta_i x_i^{\otimes d} + \mathcal{W}/\sqrt{p}$ where r is the rank of the signal of interest. In this line of work, Chen et al. (2021) proves that the asymptotic behavior of a low-rank spiked tensor model with orthogonal signal components, i.e., $\langle x_i, x_j \rangle = 0$ for $i \neq j \in [r]$, can be understood from the analysis of a rank-one model. Moreover, da Silva et al. (2015b;a) show that estimating a higher rank signal boils down to performing successive rank-one approximations using iterative tensor deflation. While the latter result provides a more tractable approach to low-rank signal recovery in the orthogonal case, it may fail in signal reconstruction in the non-orthogonal case (Seddik et al., 2022).

Other enhanced deflation techniques rely on orthogonal projections (Mackey, 2008) while exhibiting the same alteration as the standard deflation in the non-orthogonal case, as illustrated in Figure 1. The latter depicts signal recovery, in terms of alignments, from a rank-two tensor $\sum_{i=1}^2 \beta_i x_i^{\otimes 3}$ using an orthogonalized deflation (Mackey, 2008). It is clearly observed that, when $\beta_1 \approx \beta_2$, the non-orthogonality of x_1 and x_2 prevents efficient recovery. We highlight the fact that measuring alignments is a concrete performance measure of the recovery quality. Indeed, given that in high dimension, the probability that two random vectors u, v are orthogonal, i.e., $\langle u, v \rangle = 0$, showcases the difficulty of obtaining high estimation accuracies in this setting.

Key contributions: Aiming to understand the interplay of the orthogonalized tensor deflation and improve its efficiency, our key contributions can be summarized as follows:

1. We consider a slightly different orthogonalized tensor deflation algorithm by introducing a parameter γ as described in §3.2. In particular, $\gamma = 1$ corresponds to the classical orthogonalized deflation (Mackey, 2008).
2. We carry out a random tensor theory (RTT) analysis of the considered deflation method applied on a *rank-two asymmetric spiked tensor model* defined in §3.1. Spiked models are more general and offer many theoretical advantages

then considering noiseless low-rank models. For instance, subtracting a best rank-one approximation of a noiseless low-rank tensor may increase its rank (Stegeman & Comon, 2010), while spiked models do not suffer from such limitation since their noise components is full rank (Strassen, 1983).

3. Based on our theoretical analysis, we optimize the parameter γ introduced in the deflation mechanism which allows us to design a more efficient tensor deflation algorithm (see §3.3).

2. Notations and Background

The set $\{1, \dots, n\}$ is denoted by $[n]$. The unit sphere in \mathbb{R}^p is denoted by \mathbb{S}^{p-1} . The Dirac measure at some real value x is denoted by δ_x . The support of a measure μ is denoted by $\text{supp}(\mu)$. The inner-product between two vectors u, v is denoted by $\langle u, v \rangle = \sum_i u_i v_i$. The imaginary part of a complex number z is denoted by $\Im[z]$. The set of eigenvalues of a matrix M is denoted by $\text{Sp}(M)$. The almost sure converges is denoted by the arrow $\xrightarrow{\text{a.s.}}$. The notation $a_n \asymp b_n$ means that a_n and b_n converge to the same limit as $n \rightarrow \infty$.

2.1. Tensor Notations and Contractions

In this section, we provide the main tensor notations and definitions used throughout the paper, which we recommend to follow carefully for better understanding of our paper.

Three-order tensors: The set of three-order tensors of size p is denoted $\mathbb{R}^{p \times p \times p}$. The scalar T_{ijk} or $[\mathcal{T}]_{ijk}$ denotes the (i, j, k) entry of a tensor $\mathcal{T} \in \mathbb{R}^{p \times p \times p}$. In the remainder, we will mainly consider tensors from $\mathbb{R}^{p \times p \times p}$, and for brevity, we may omit the notation $\mathcal{T} \in \mathbb{R}^{p \times p \times p}$.

Rank- r tensors: A tensor \mathcal{T} is said to be of rank-one if it can be represented as the outer product of three real-valued vectors $x, y, z \in \mathbb{R}^p$. In this case, we write $\mathcal{T} = x \otimes y \otimes z$, where the outer product is defined such that $[x \otimes y \otimes z]_{ijk} = x_i y_j z_k$. More generally, a tensor \mathcal{T} is of rank- r , for some integer r , if it can be expressed as the sum of r rank-one terms, written as $\mathcal{T} = \sum_{i=1}^r x_i \otimes y_i \otimes z_i$, where $x_i, y_i, z_i \in \mathbb{R}^p$ for all $i \in [r]$. To maintain consistency, we will adhere to the convention of using x_i or u_i to represent the components of the first mode, y_i or v_i to represent the components of the second mode, and z_i or w_i to represent the components of the third mode throughout the paper.

Tensor contractions: The first mode contraction of a tensor \mathcal{T} with a vector x results in a matrix denoted $\mathcal{T}(x, \cdot, \cdot)$ with entries $[\mathcal{T}(x, \cdot, \cdot)]_{jk} = \sum_{i=1}^p x_i T_{ijk}$. Similarly, $\mathcal{T}(\cdot, y, \cdot)$ and $\mathcal{T}(\cdot, \cdot, z)$ denote the second and third mode contractions of \mathcal{T} with vectors y and z respectively. We will sometimes denote these contractions by $\mathcal{T}(x)$, $\mathcal{T}(y)$ and $\mathcal{T}(z)$ if there is no ambiguity. The contraction of \mathcal{T} on two vectors x, y is a vector denoted $\mathcal{T}(x, y, \cdot)$ with entries $[\mathcal{T}(x, y, \cdot)]_k = \sum_{ij} x_i y_j T_{ijk}$. The contraction of \mathcal{T} on three vectors x, y, z is a scalar denoted $\mathcal{T}(x, y, z) = \sum_{ijk} x_i y_j z_k T_{ijk}$. The first mode contraction of \mathcal{T} with a matrix $M \in \mathbb{R}^{p \times p}$ results in a tensor denoted $\mathcal{T} \times_1 M$ with entries $[\mathcal{T} \times_1 M]_{ijk} = \sum_{i'=1}^p M_{ii'} T_{i'jk}$. Similarly, $\mathcal{T} \times_2 N$ and $\mathcal{T} \times_3 P$ denote the second and third modes tensor-matrix contractions of the tensor \mathcal{T} with the matrices N and P respectively. The notation $u \otimes M$ stands for the tensor with entries $u_i M_{jk}$.

Tensor norms: The Frobenius norm of a tensor \mathcal{T} is denoted $\|\mathcal{T}\|_F$ with $\|\mathcal{T}\|_F^2 = \sum_{ijk} T_{ijk}^2$. The spectral norm of \mathcal{T} is $\|\mathcal{T}\| = \sup_{u, v, w \in \mathbb{S}^{p-1}} |\mathcal{T}(u, v, w)|$.

Best rank-one approximation and tensor power iteration: A best rank-one approximation of \mathcal{T} corresponds to a rank-one tensor $\lambda u \otimes v \otimes w$, where $\lambda > 0$ and u, v, w are unitary vectors, that minimizes the square loss $\|\mathcal{T} - \lambda u \otimes v \otimes w\|_F^2$. The latter generalizes to tensors the concept of singular value and vectors (Lim, 2005) and the scalar λ coincides with the spectral norm of \mathcal{T} . In particular, the quadruple (λ, u, v, w) satisfies the following identities

$$\mathcal{T}(\cdot, v, w) = \lambda u, \quad \mathcal{T}(u, \cdot, w) = \lambda v, \quad \mathcal{T}(u, v, \cdot) = \lambda w, \quad \lambda = \mathcal{T}(u, v, w). \quad (1)$$

Such a best rank-one approximation can be computed via *tensor power iteration* which consists in iterating

$$u \leftarrow \frac{\mathcal{T}(\cdot, v, w)}{\|\mathcal{T}(\cdot, v, w)\|} \quad v \leftarrow \frac{\mathcal{T}(u, \cdot, w)}{\|\mathcal{T}(u, \cdot, w)\|} \quad w \leftarrow \frac{\mathcal{T}(u, v, \cdot)}{\|\mathcal{T}(u, v, \cdot)\|}$$

starting from some initialization (Anandkumar et al., 2014).

2.2. Random Matrix Theory

In this section, we provide some necessary tools from random matrix theory (RMT) which are at the core of our main results. Specifically, we will consider the *resolvent* formalism (Hachem et al., 2007) which allows one to characterize the spectral behavior of large symmetric random matrices. Given a symmetric matrix $\mathbf{S} \in \mathbb{R}^{n \times n}$, the resolvent of \mathbf{S} is defined as $\mathbf{R}(z) = (\mathbf{S} - z\mathbf{I}_n)^{-1}$ for $z \in \mathbb{C} \setminus \text{Sp}(\mathbf{S})$.

In essence, RMT focuses on describing the distribution of eigenvalues of large random matrices. Typically, under certain technical assumptions on some random matrix $\mathbf{S} \in \mathbb{R}^{n \times n}$ with eigenvalues $\lambda_1, \dots, \lambda_n$, the *empirical spectral measure* of \mathbf{S} , defined as $\hat{\mu} = \frac{1}{n} \sum_{i=1}^n \delta_{\lambda_i}$, converges in the weak sense (Van Der Vaart & Wellner, 1996) to some deterministic probability measure μ as $n \rightarrow \infty$ and RMT aims at describing such μ . To this end, one of the widely considered approaches relies on the *Stieltjes transform* (Tao, 2012). Given a probability measure μ , the Stieltjes transform of μ is defined as $g_\mu(z) = \int \frac{d\mu(\lambda)}{\lambda - z}$ with $z \in \mathbb{C} \setminus \text{supp}(\mu)$, and the inverse formula allows one to describe the density function of μ as $\mu(dx) = \frac{1}{\pi} \lim_{\varepsilon \rightarrow 0} \Im[g_\mu(x + i\varepsilon)]$.

The Stieltjes transform of the empirical spectral measure, $\hat{\mu}$, is closely related to the resolvent of \mathbf{S} through the normalized trace operator. In fact, $g_{\hat{\mu}}(z) = \frac{1}{n} \text{tr} \mathbf{R}(z)$ and the *almost sure* convergence of $g_{\hat{\mu}}(z)$ to some deterministic Stieltjes transform $g(z)$ is equivalent to the weak convergence between the underlying probability measures (Tao, 2012). Our analysis relies on estimating quantities involving $\frac{1}{n} \text{tr} \mathbf{R}(z)$, making the use of the resolvent approach a natural choice.

3. Model & Main Results

3.1. Rank-two Spiked Tensor Model

We consider the following rank-two spiked tensor model

$$\mathcal{T}_1 \equiv \mathcal{S} + \frac{1}{\sqrt{n}} \mathcal{W} \in \mathbb{R}^{p \times p \times p}, \quad (2)$$

where $\mathcal{S} = \sum_{i=1}^2 \beta_i x_i \otimes y_i \otimes z_i$, $\beta_i \geq 0$ correspond to the signal-to-noise ratios (SNRs), $x_i, y_i, z_i \in \mathbb{S}^{p-1}$ are the signal components, \mathcal{W} is a random tensor with standard Gaussian i.i.d. entries, i.e., $W_{ijk} \sim \mathcal{N}(0, 1)$, and $n = 3p$.

We further consider that the between signal components alignments are uniform across the modes, i.e.

$$\alpha \equiv \langle x_1, x_2 \rangle = \langle y_1, y_2 \rangle = \langle z_1, z_2 \rangle. \quad (3)$$

The parameter α will therefore control the correlation between the rank-two terms. Specifically, $\alpha = 0$ corresponds to the orthogonal case while $\alpha > 0$ models the correlated case. In the following we denote $\alpha_{ij} = \alpha$ if $i \neq j$ and 1 otherwise. Our results can be easily extended to higher ranks and high order tensors but we consider the above model and restricted assumption in (3) for the sake of simplicity.

3.2. RTT Analysis of Orthogonalized Tensor Deflation

In order to recover the signal components, we first consider a best rank-one approximation $\hat{\lambda}_1 \hat{u}_1 \otimes \hat{v}_1 \otimes \hat{w}_1$ of the tensor \mathcal{T}_1 as a *first deflation step*. Given the vector $\hat{u}_1 \in \mathbb{S}^{p-1}$, the *second deflation step* consists in performing a best rank-one approximation $\hat{\lambda}_2 \hat{u}_2 \otimes \hat{v}_2 \otimes \hat{w}_2$ of the following tensor

$$\mathcal{T}_2 \equiv \mathcal{T}_1 \times_1 (\mathbf{I}_p - \gamma \hat{u}_1 \hat{u}_1^\top) = \mathcal{T}_1 - \gamma \hat{u}_1 \otimes \mathcal{T}_1(\hat{u}_1), \quad (4)$$

for some parameter $\gamma \in [0, 1]$ which we will optimize based on our theoretical analysis. In particular, when $\gamma = 1$, the tensor \mathcal{T}_2 is obtained as the orthogonal projection of the first mode of the tensor \mathcal{T}_1 on the hyperplane defined by the plane normal vector \hat{u}_1 , which corresponds to the classical *orthogonalized deflation* (Mackey, 2008).

Moreover, as we recalled in (1), the best rank-one approximations $\hat{\lambda}_1 \hat{u}_1 \otimes \hat{v}_1 \otimes \hat{w}_1$ and $\hat{\lambda}_2 \hat{u}_2 \otimes \hat{v}_2 \otimes \hat{w}_2$ of \mathcal{T}_1 and \mathcal{T}_2 respectively satisfy the following identities, for $i \in [2]$

$$\mathcal{T}_i(\cdot, \hat{v}_i, \hat{w}_i) = \hat{\lambda}_i \hat{u}_i, \quad \mathcal{T}_i(\hat{u}_i, \cdot, \hat{w}_i) = \hat{\lambda}_i \hat{v}_i, \quad \mathcal{T}_i(\hat{u}_i, \hat{v}_i, \cdot) = \hat{\lambda}_i \hat{w}_i, \quad \hat{\lambda}_i = \mathcal{T}_i(\hat{u}_i, \hat{v}_i, \hat{w}_i). \quad (5)$$

In the remainder, we compute $\hat{\lambda}_1 \hat{u}_1 \otimes \hat{v}_1 \otimes \hat{w}_1$ and $\hat{\lambda}_2 \hat{u}_2 \otimes \hat{v}_2 \otimes \hat{w}_2$ in all our simulations via tensor power iteration initialized with tensor SVD (Auddy & Yuan, 2022), which has been proven to converge in polynomial time for $\beta_i \geq O(p^{3/2})$ in the

orthogonal case $\alpha = 0$. Moreover, for each $i \in [2]$, denote the following alignments as

$$\begin{aligned}\hat{\rho}_{1i} &\equiv |\langle \hat{u}_1, x_i \rangle| \asymp |\langle \hat{v}_1, y_i \rangle| \asymp |\langle \hat{w}_1, z_i \rangle|, \\ \hat{\theta}_{2i} &\equiv |\langle \hat{u}_2, x_i \rangle|, \quad \hat{\rho}_{2i} \equiv |\langle \hat{v}_2, y_i \rangle| \asymp |\langle \hat{w}_2, z_i \rangle|, \\ \hat{\kappa} &\equiv |\langle \hat{u}_1, \hat{u}_2 \rangle|, \quad \hat{\eta} \equiv |\langle \hat{v}_1, \hat{v}_2 \rangle| \asymp |\langle \hat{w}_1, \hat{w}_2 \rangle|.\end{aligned}\tag{6}$$

The equivalences $|\langle \hat{u}_1, x_i \rangle| \asymp |\langle \hat{v}_1, y_i \rangle| \asymp |\langle \hat{w}_1, z_i \rangle|$, $|\langle \hat{v}_2, y_i \rangle| \asymp |\langle \hat{w}_2, z_i \rangle|$ and $|\langle \hat{v}_1, \hat{v}_2 \rangle| \asymp |\langle \hat{w}_1, \hat{w}_2 \rangle|$ are a consequence of our assumption in (3) and since all the mode dimensions of \mathcal{T}_1 are equal. Moreover, $\hat{\theta}_{2i} \not\asymp \hat{\rho}_{2i}$ and $\hat{\kappa} \not\asymp \hat{\eta}$ since the projection in (4) is applied only on the first mode.

In order to decipher the asymptotic behavior of the considered deflation method as $n \rightarrow \infty$, our main goal is to compute the asymptotic expected values of the singular values λ_i and the alignments $\hat{\rho}_{1i}$, $\hat{\theta}_{2i}$, $\hat{\rho}_{2i}$, $\hat{\kappa}$, $\hat{\eta}$. Indeed, using concentration arguments one can show that these quantities tend to concentrate around their expected values as n grows large with variances of order $O(n^{-1})$, in the same vein as (Benaych-Georges et al., 2011) which studied the fluctuations of the largest eigenvalues of large random matrices.

Moreover, we also address the problem of estimating the underlying model parameters, namely the signal-to-noise ratios β_1, β_2 and the correlation parameter α based on a single realization of \mathcal{T}_1 . This allows us to design an improved deflation algorithm in the correlated case. Our analysis relies on a recently developed random tensor theory approach from (Seddik et al., 2021). In particular, we analyze the random tensor model obtained at each deflation step by: **1)** Identifying a corresponding random matrix; **2)** Describing the limiting spectral measure of the latter and **3)** Computing the asymptotic singular value and corresponding alignments.

3.2.1. FIRST DEFLATION STEP

We start by analyzing the random tensor model of the first deflation step, namely the tensor \mathcal{T}_1 in (2).

Corresponding Random Matrix Model: Starting from the identities in (5) for $i = 1$, it has been shown in (Seddik et al., 2021) that the study of the random tensor \mathcal{T}_1 and its associated singular value and vectors $(\hat{\lambda}_1, \hat{u}_1, \hat{v}_1, \hat{w}_1)$ boils down to the analysis of the following block-wise contraction random matrix of size $n \times n$ (see Appendix 7.1)

$$\mathbf{N} \equiv \frac{1}{\sqrt{n}} \begin{pmatrix} 0 & \mathcal{W}(\hat{w}_1) & \mathcal{W}(\hat{v}_1) \\ \mathcal{W}(\hat{w}_1)^\top & 0 & \mathcal{W}(\hat{u}_1) \\ \mathcal{W}(\hat{v}_1)^\top & \mathcal{W}(\hat{u}_1)^\top & 0 \end{pmatrix}.\tag{7}$$

Limiting Spectral Measure: In fact, the characterization of the limits of λ_1 and the alignments $\hat{\rho}_{1i}$ for $i \in [2]$ when $n \rightarrow \infty$ boils down to the computation of the Stieltjes transform of the limiting spectral measure of the random matrix \mathbf{N} , see Appendix 7.1.2 for details. We henceforth need the following technical assumptions to characterize such Stieltjes transform.

Assumption 3.1. As $n \rightarrow \infty$, there exists a sequence of critical points $(\hat{\lambda}_1, \hat{u}_1, \hat{v}_1, \hat{w}_1)$ such that $\hat{\lambda}_1 \xrightarrow{\text{a.s.}} \lambda_1 > 2\sqrt{\frac{2}{3}}$ and $\hat{\rho}_{1i} \xrightarrow{\text{a.s.}} \rho_{1i} > 0$.

Under Assumption 3.1, we have the following result from (Seddik et al., 2021, Corollary 1) which characterizes the limiting spectral measure of the random matrix \mathbf{N} .

Theorem 3.2. Under Assumption 3.1, the spectral measure of \mathbf{N} converges weakly to a semi-circle law μ of compact support $[-2\sqrt{\frac{2}{3}}, 2\sqrt{\frac{2}{3}}]$ and density function $\mu(dx) = \frac{3}{4\pi} \sqrt{(x^2 - \frac{8}{3})^+}$. Moreover, the Stieltjes transform of μ is

$$r(z) = \frac{3}{4} \left(-z + \sqrt{z^2 - \frac{8}{3}} \right), \quad \text{for } z > 2\sqrt{\frac{2}{3}}.$$

Figure 2 depicts the histogram of the eigenvalues of \mathbf{N} and the corresponding limiting semi-circle law as per Theorem 3.2. Note that the spectral measure of \mathbf{N} is not affected by the parameters β_1, β_2 and α but some conditions are required on the latest to ensure Assumption 3.1 as we will see subsequently. We also refer the reader to (Goulart et al., 2021; Seddik et al., 2021) for a more detailed discussion on Assumption 3.1 in the rank-one case.

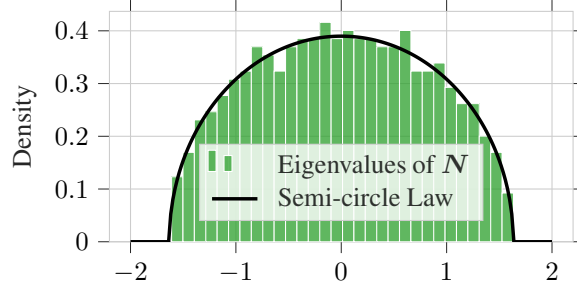


Figure 2. Histogram of the eigenvalues of N and limiting semi-circle law from Theorem 3.2. We considered $p = 200$, $\beta_1 = 20$, $\beta_2 = 15$, $\alpha = 0.8$ and one realization of \mathcal{T}_1 .

Asymptotic Singular Value and Alignments: We now consider the computation of λ_1 to give an insight about Assumption 3.1. Given Theorem 3.2, one can derive by taking the expectation w.r.t. \mathcal{W} of the identity $\hat{\lambda}_1 = \mathcal{T}_1(\hat{u}_1, \hat{v}_1, \hat{w}_1)$ in (5), that the limiting singular value λ_1 satisfies the following equation (see Appendix 7.1.2 for the derivations)

$$\lambda_1 + r(\lambda_1) = \sum_{i=1}^2 \beta_i \rho_{1i}^3. \quad (8)$$

Therefore, since the Stieltjes transform r has to be evaluated in λ_1 , the latter must lie outside the support of μ which is ensured by Assumption 3.1 if the signal strengths β_1 or β_2 are sufficiently high. In the case $\alpha = 0$, it was shown in (Seddik et al., 2021, Corollary 3) that $\max\{\beta_1, \beta_2\}$ must be greater than $\frac{2\sqrt{3}}{3}$ to ensure $\lambda_1 > 2\sqrt{\frac{2}{3}}$. Besides, note that when $\lambda_1 \leq 2\sqrt{\frac{2}{3}}$, i.e., λ_1 lies inside the support of μ , it basically corresponds to the case where the tensor \mathcal{T}_1 is indistinguishable from its noise counterpart \mathcal{W} , and hence recovering the signal components is information-theoretically impossible (Richard & Montanari, 2014; Lesieur et al., 2017; Jagannath et al., 2020; Goulart et al., 2021; Seddik et al., 2021).

Taking the expectation w.r.t. \mathcal{W} of the remaining identities in (5) for $i = 1$, projected on the signal components x_i, y_i, z_i for $i \in [2]$ as detailed in Appendix 7.1.3, allows us to obtain the following result which characterizes the asymptotic behavior of the first deflation step.

Theorem 3.3. *Under Assumption 3.1, the limiting singular value λ_1 and corresponding alignments ρ_{1i} for $i \in [2]$ of the first deflation step satisfy the following system of equations*

$$\begin{cases} f_r(\lambda_1) = \sum_{i=1}^2 \beta_i \rho_{1i}^3, \\ h_r(\lambda_1) \rho_{1j} = \sum_{i=1}^2 \beta_i \alpha_{ij} \rho_{1i}^2 \quad \text{for } j \in [2], \end{cases} \quad (9)$$

where we recall $\alpha_{ij} = \alpha$ if $i \neq j$ and 1 otherwise, and we denoted $f_r(z) = z + r(z)$ and $h_r(z) = -\frac{1}{r(z)}$.

Proof. See Appendices 7.1.2 and 7.1.3. □

Figure 3 shows the simulated versus asymptotic singular value and alignments of the first deflation step as stated by Theorem 3.3. Specifically, the asymptotic behavior of the first deflation step is described by a set of three polynomial equations involving λ_1 and ρ_{1i} for $i \in [2]$. The existence and uniqueness of such solutions is not addressed in our present analysis and we stress out that the asymptotic curves in Figure 3 are obtained by solving numerically the system (9) initialized with the simulated singular value and alignments from one realization of the random tensor \mathcal{T}_1 .

3.2.2. SECOND DEFLATION STEP

We henceforth turn into the description of the second deflation step asymptotics.

Corresponding Random Matrix Model: Denote $\hat{u}_3 = \hat{u}_2 - \gamma \langle \hat{u}_1, \hat{u}_2 \rangle \hat{u}_1$. We show in Appendix 7.2 that the study of the second deflation step boils down to the analysis of the following $n \times n$ block-wise contraction random matrix

$$M \equiv \frac{1}{\sqrt{n}} \begin{pmatrix} 0 & \mathcal{W}(\hat{w}_2) & \mathcal{W}(\hat{v}_2) \\ \mathcal{W}(\hat{w}_2)^\top & 0 & \mathcal{W}(\hat{u}_3) \\ \mathcal{W}(\hat{v}_2)^\top & \mathcal{W}(\hat{u}_3)^\top & 0 \end{pmatrix}, \quad (10)$$

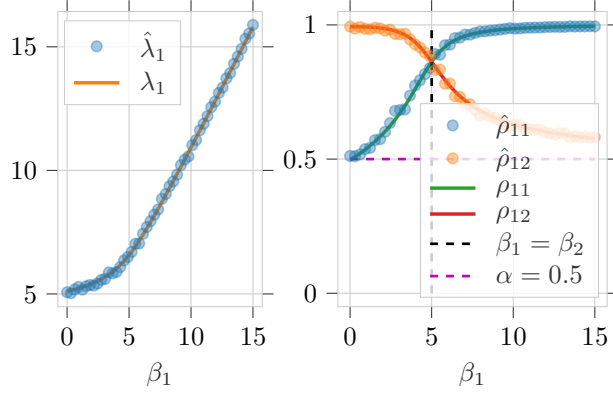


Figure 3. Simulated versus asymptotic singular value and alignments corresponding to the first deflation step as per Theorem 3.3. We considered $\beta_1 = 5$, $\alpha = 0.5$, $p = 100$ and varying $\beta_1 \in [0, 15]$. The system of equations in (9) is solved numerically and initialized with the simulated singular value and alignments (dotted curves) from one realization of \mathcal{T}_1 .

Limiting Spectral Measure: We demonstrate that for some $\gamma \neq 1$, the limiting spectral measure of \mathbf{M} does not follow a semi-circle law due to the additional term $\gamma \langle \hat{u}_1, \hat{u}_2 \rangle \mathcal{W}(\hat{u}_1)$ induced by the correlation between the singular vectors \hat{u}_1 and \hat{u}_2 . Besides, when $\gamma = 0$ or $\gamma = 1$, the term $\gamma \langle \hat{u}_1, \hat{u}_2 \rangle \mathcal{W}(\hat{u}_1)$ vanishes in which cases the limiting spectral measure of \mathbf{M} is again described by the semi-circle law in Theorem 3.2. In fact, when $\gamma = 1$, we have from the identity $\mathcal{T}_2(\cdot, \hat{v}_2, \hat{w}_2) = \hat{\lambda}_2 \hat{u}_2$ in (5) and given \mathcal{T}_2 in (4)

$$\lambda_2 \langle \hat{u}_1, \hat{u}_2 \rangle = \mathcal{T}_2(\hat{u}_1, \hat{v}_2, \hat{w}_2) = \mathcal{T}_1(\hat{u}_1, \hat{v}_2, \hat{w}_2) - \underbrace{\langle \hat{u}_1, \hat{u}_1 \rangle}_{=1} \mathcal{T}_1(\hat{u}_1, \hat{v}_2, \hat{w}_2) = 0, \quad (11)$$

which implies $\langle \hat{u}_1, \hat{u}_2 \rangle = 0$ since the spectral norm of the tensor \mathcal{T}_2 is not null, due to the presence of the noise term.

We therefore provide the result characterizing the limiting spectral measure of \mathbf{M} for any $\gamma \in [0, 1]$, and which in turn generalizes Theorem 3.2 to random contraction matrices of the form in (10). We start by the following definition.

Definition 3.4. Let ν be the probability measure with Stieltjes transform $q(z) = a(z) + 2b(z)$ verifying $\Im[q(z)] > 0$ for $\Im[z] > 0$, where $a(z)$ and $b(z)$ satisfy the following system of equations, for $z \notin \text{supp}(\nu)$

$$\begin{cases} [2b(z) + z] a(z) + \frac{1}{3} = 0, \\ (a(z) + z - \tau b(z)) b(z) + \frac{1}{3} = 0, \end{cases} \quad (12)$$

for some parameter $\tau \in \mathbb{R}$. Moreover, the density function corresponding to ν is given by the Stieltjes inverse formula $\nu(dx) = \frac{1}{\pi} \lim_{\varepsilon \rightarrow 0} \Im[q(x + i\varepsilon)]$.

Similarly to the analysis of the first deflation step, we need some additional technical assumptions to describe the limiting singular value λ_2 and corresponding alignments.

Assumption 3.5. As $n \rightarrow \infty$, there exists a sequence of critical points $(\hat{\lambda}_2, \hat{u}_2, \hat{v}_2, \hat{w}_2)$ such that, for $i \in [2]$

$$\hat{\lambda}_2 \xrightarrow{\text{a.s.}} \lambda_2, \quad \hat{\theta}_{2i} \xrightarrow{\text{a.s.}} \theta_{2i}, \quad \hat{\kappa} \xrightarrow{\text{a.s.}} \kappa, \quad \hat{\rho}_{2i} \xrightarrow{\text{a.s.}} \rho_{2i}, \quad \hat{\eta} \xrightarrow{\text{a.s.}} \eta,$$

where $\lambda_2 \notin \text{supp}(\nu)$ with ν defined in Definition 3.4 for $\tau = \gamma\kappa^2 - 1 + \kappa(\gamma - 1)$ and suppose $\theta_{2i}, \kappa, \rho_{2i}, \eta > 0$.

We therefore have the following theorem which characterizes the limiting spectral measure of \mathbf{M} .

Theorem 3.6. Under Assumption 3.5, the spectral measure of \mathbf{M} converges weakly to the probability measure ν defined in Definition 3.4 for $\tau = \gamma\kappa^2 - 1 + \kappa(\gamma - 1)$.

Proof. See Appendix 7.2.1. □

In essence, if the involved alignments in the second deflation step converge asymptotically, Theorem 3.6 states the convergence of the spectral measure of \mathbf{M} to the deterministic measure ν defined in Definition 3.4 for $\tau = \gamma\kappa^2 - 1 + \kappa(\gamma - 1)$.

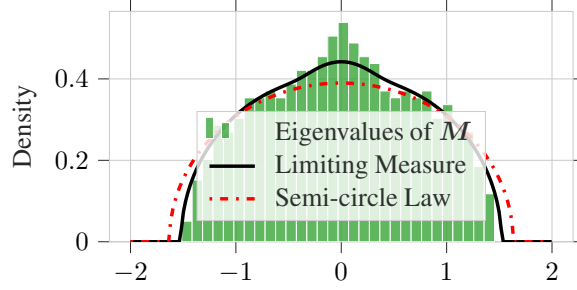


Figure 4. Histogram of the eigenvalues of M and corresponding limiting spectral measure as per Theorem 3.6. We considered $p = 200$, $\beta_1 = 20$, $\beta_2 = 15$, $\alpha = 0.8$, $\gamma = 0.85$ and one realization of \mathcal{T}_1 .

$$\begin{cases} f_q(\lambda_2) - \frac{\gamma\kappa\eta^2}{3}r(\lambda_1) - 2\gamma\kappa^2b(\lambda_2) = \sum_{i=1}^2 \beta_i\theta_{2i}\rho_{2i}^2 - \gamma\kappa \sum_{i=1}^2 \beta_i\rho_{1i}\rho_{2i}^2, \\ [f_q(\lambda_2) - a(\lambda_2)]\theta_{2j} - \gamma\rho_{1j} \left[\frac{\eta^2}{3}r(\lambda_1) + 2\kappa b(\lambda_2) \right] = \sum_{i=1}^2 \beta_i\alpha_{ij}\rho_{2i}^2 - \gamma\rho_{1j} \sum_{i=1}^2 \beta_i\rho_{1i}\rho_{2i}^2 \quad \text{for } j \in [2], \\ [\lambda_2 + 2(1 - \gamma)b(\lambda_2)]\kappa = (1 - \gamma) \left[\sum_{i=1}^2 \beta_i\rho_{1i}\rho_{2i}^2 - \frac{\eta^2}{3}r(\lambda_1) \right], \\ [f_q(\lambda_2) - (1 + \gamma\kappa^2)b(\lambda_2)]\rho_{2j} = \sum_{i=1}^2 \beta_i\theta_{2i}\rho_{2i}\alpha_{ij} - \gamma\kappa \left[\sum_{i=1}^2 \beta_i\rho_{1i}\rho_{2i}\alpha_{ij} - \frac{\rho_{1j}\eta}{3}r(\lambda_1) \right] \quad \text{for } j \in [2], \\ [\lambda_2 + a(\lambda_2) + (1 - \gamma\kappa^2)b(\lambda_2) - \frac{\gamma\kappa}{3}r(\lambda_1)]\eta = \sum_{i=1}^2 \beta_i\theta_{2i}\rho_{1i}\rho_{2i} - \gamma\kappa \sum_{i=1}^2 \beta_i\rho_{1i}^2\rho_{2i}. \end{cases} \quad (14)$$

We particularly recall that κ corresponds to the limit of $\langle \hat{u}_1, \hat{u}_2 \rangle$, which highlights the fact that the spectrum of M can be deformed if the singular vectors u_1 and u_2 are correlated, i.e., if $\gamma \neq 1$. This phenomenon is depicted in Figure 4 where we see that for $\gamma = 0.85$, the limiting spectral measure of M defers from the semi-circle law. In contrast, if $\gamma = 1$ we have $\kappa = 0$ as we saw in (43) which implies that $\tau = -1$. In this case, the limiting spectral measure ν becomes equal to μ , thereby describing again a semi-circle law. This can be trivially checked from Definition 3.4 by setting $\tau = -1$ and $a(z) = b(z)$, and we therefore find $a(z) = b(z) = \frac{r(z)}{3}$ and $q(z) = r(z)$. Note that for $\gamma \in (0, 1)$, the Stieltjes transform $q(z)$ can be computed numerically by alternating the equations in (12) as per Algorithm 1, which can be proved to converge to a fixed point in the same vein as (Louart & Couillet, 2018).

Asymptotic Singular Value and Alignments: As for the first deflation step, taking the expectation w.r.t. \mathcal{W} of the identity $\hat{\lambda}_2 = \mathcal{T}_2(\hat{u}_2, \hat{v}_2, \hat{w}_2)$ in (5) allows us to obtain the equation satisfied by λ_2 , see Appendix 7.2.2, which yields

$$f_q(\lambda_2) - \frac{\gamma\kappa\eta^2}{3}r(\lambda_1) - 2\gamma\kappa^2b(\lambda_2) = \sum_{i=1}^2 \beta_i\theta_{2i}\rho_{2i}^2 - \gamma\kappa \sum_{i=1}^2 \beta_i\rho_{1i}\rho_{2i}^2, \quad (13)$$

where $f_q(z) = z + q(z)$. Again, the limiting singular value λ_2 must lie outside the support of ν , as we assumed in Assumption 3.5, since its corresponding Stieltjes transform $q(z)$ (and the function $b(\cdot)$) needs to be evaluated at λ_2 . In fact, if $\lambda_2 \in \text{supp}(\nu)$, then it is information-theoretically impossible to recover the second signal term (i.e., the one with strength $\min\{\beta_1, \beta_2\}$).

Moreover, taking the expectation w.r.t. \mathcal{W} of the remaining identities in (5) for $i = 2$, projected on the signal components x_i, y_i, z_i for $i \in [2]$ and the first singular vectors u_1, v_1, w_1 , allows us to derive the result characterizing the behavior of the second deflation step.

Theorem 3.7. *Under Assumption 3.5, the limiting singular value λ_2 and corresponding alignments θ_{2i}, ρ_{2i} for $i \in [2]$ and κ, η of the second deflation step satisfy the system of equations in (14).*

Proof. See Appendices 7.2.2 and 7.2.3. □

Figure 7 depicts the simulated singular value and alignments of the second deflation step and their asymptotic counterparts as given by Theorem 3.7. In essence, the asymptotic behavior of the second deflation step is described by a set of seven polynomial equations in λ_2 and the alignments $\theta_{2i}, \rho_{2i}, \kappa$ and η . Again, we do not address the existence and uniqueness of such solutions, and we solve the system in (14) numerically starting from the simulated singular value and alignments from one realization of \mathcal{T}_1 . Contrarily to the first deflation step, we highlight that the Stieltjes transform $q(z)$ depends on the alignment κ . Therefore, we alternate solving the system in (14) with the fixed point equations in (12) for $\tau = \gamma\kappa^2 - 1 + \kappa(\gamma - 1)$ as per Theorem 3.6.

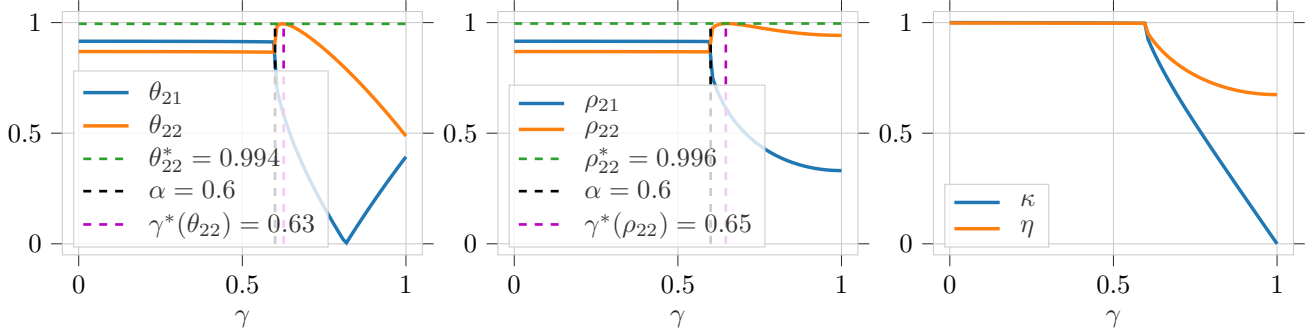


Figure 5. Asymptotic alignments of the second deflation varying the hyper-parameter γ . We considered $\beta_1 = 10$, $\beta_2 = 8$ and $\alpha = 0.6$.

We further stress out that for a fixed β_2 large enough and $\alpha \neq 1$, there exists a threshold for β_1 below which it is information-theoretically impossible to recover the second signal component. This can be visible from Figure 7 for $\beta_1 \approx 2$, below which all the alignments are asymptotically null and the asymptotic singular value converges to the right edge of the distribution ν . Precisely, this corresponds to the scenario where Assumption 3.5 is not verified. Moreover, not that there might also exist a theoretical-algorithmic spectral gap, that needs to be determined for the present deflation procedure, in the same vein as in (Richard & Montanari, 2014) for the rank-one case.

Case $\gamma = 1$: As we discussed earlier, in the case $\gamma = 1$ the limiting spectral measure ν becomes equal to the semi-circle law μ described in the first deflation step. Moreover, the system of equations in (14) reduces to the following equations, for $j \in [2]$, which will be needed subsequently.

$$\begin{cases} f_r(\lambda_2) = \sum_{i=1}^2 \beta_i \theta_{2i} \rho_{2i}^2 \\ h_r(\lambda_2) \theta_{2j} - \frac{\eta^2}{3} r(\lambda_1) \rho_{1j} = \sum_{i=1}^2 \beta_i \alpha_{ij} \rho_{2i}^2 - \rho_{1j} \sum_{i=1}^2 \beta_i \rho_{1i} \rho_{2i}^2 \\ h_r(\lambda_2) \rho_{2j} = \sum_{i=1}^2 \beta_i \theta_{2i} \rho_{2i} \alpha_{ij} \\ [\lambda_2 + \frac{2}{3} r(\lambda_2)] \eta = \sum_{i=1}^2 \beta_i \theta_{2i} \rho_{1i} \rho_{2i} \end{cases} \quad (15)$$

3.2.3. MODEL PARAMETERS ESTIMATION

In this section, we discuss the problem of estimating the underlying model parameters, namely the SNRs and the signal components correlation $\beta \equiv (\beta_1, \beta_2, \alpha) \in \mathbb{R}^3$, and the alignments $\rho \equiv (\rho_{1i}, \rho_{2i}, \theta_{2i} \mid i \in [2]) \in \mathbb{R}^6$ from one realization of the random tensor \mathcal{T}_1 . Indeed, this will allow us to design an improved deflation algorithm by optimizing the parameter γ introduced in the second deflation step. Further denoting $\lambda \equiv (\lambda_1, \lambda_2, \eta) \in \mathbb{R}^3$, we define the mapping $\psi : \mathbb{R}^3 \times \mathbb{R}^3 \times \mathbb{R}^6 \rightarrow \mathbb{R}^9$ through (16), where the first three entries of the vector $\psi(\beta, \lambda, \rho)$ correspond to the first deflation step equations in (9) while the remaining entries correspond to the second deflation step for $\gamma = 1$ characterized by (15). In particular, the singular values λ_1, λ_2 and the corresponding alignments satisfy $\psi(\beta, \lambda, \rho) = 0$. On the other hand, given an estimate $\hat{\lambda} = (\hat{\lambda}_1, \hat{\lambda}_2, \hat{\eta})$ of λ , which can be computed via tensor power iteration as discussed previously, we can solve $\psi(\cdot, \hat{\lambda}, \cdot) = 0$ in the variables β and ρ while fixing $\hat{\lambda}$, which allows us to estimate the model parameters $\hat{\beta}$ and $\hat{\rho}$. In particular, Figure 9 supports this statement where we see that solving $\psi(\cdot, \hat{\lambda}, \cdot) = 0$ allows us to estimate β_1 and β_2 with reasonably low variance. Further details are deferred to Appendix 5.2.

3.3. RTT-Improved Tensor Deflation Algorithm

We are now in place to describe our improved tensor deflation algorithm. Our principal insight lies in the fact that, for $\beta_1 > \beta_2$ for instance, the asymptotic alignments θ_{22} and ρ_{22} at the second deflation step are concave functions of the parameter γ as depicted in Figure 5 for $\alpha = 0.6$ and Figure 8 for different values of α . Therefore, there exists an optimal value γ^* which maximizes such alignments and which we need to tune in order to recover the signal components efficiently, given only one realization of the spiked random tensor \mathcal{T}_1 . To this end, we propose the following procedure, which is deferred in the Appendix in Algorithm 2 due to space limitation:

- First we perform a standard orthogonalized tensor deflation with $\gamma = 1$ which corresponds to the steps 1 and 2 of Algorithm 2.

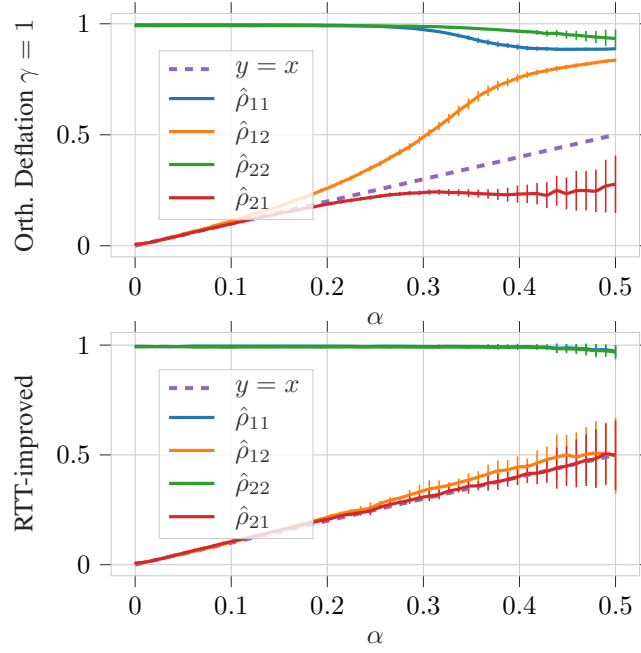


Figure 6. Alignments of first and second deflation steps in terms of α . (top) Performance of standard orthogonalized deflation ($\gamma = 1$) and (bottom) of the RTT-improved orthogonalized deflation Algorithm 2. We considered $\beta_1 = 6$, $\beta_2 = 5.7$ and $p = 150$. The curves are obtained by averaging over 200 realizations of \mathcal{T}_1 and we depict the means and std of the different alignments.

- Then we estimate the underlying model parameters, i.e., β_1, β_2 and α as we discussed in Section 3.2.3. This corresponds to the steps 3 and 4 of Algorithm 2.
- In order to find the optimal parameter γ^* which maximizes the alignment $\hat{\rho}_{22}$ for instance. We update γ as $\gamma \leftarrow \gamma - \epsilon$ for some small step size $\epsilon > 0$ and starting from $\gamma = 1$, while solving the system in (14) to get an estimation for $\hat{\rho}_{22}$. We stop updating γ until the maximum value of $\hat{\rho}_{22}$ is reached and we return the corresponding γ as γ^* . Note that at each iteration, the system in (14) is solved numerically and initialized with the previous iteration estimates. This corresponds to the steps 5-12 in Algorithm 2.
- We then perform orthogonalized deflation with γ^* along the modes 1 and 2 which provides better estimation of the signal component denoted as $\hat{\lambda}_2 \hat{u}_2^* \otimes \hat{v}_2^* \otimes \hat{w}_2^*$. This corresponds to steps 13 and 14 of Algorithm 2.
- Finally in step 15 of Algorithm 2, we re-estimate the first signal component by performing a best rank-one approximation of $\mathcal{T}_1 - \min\{\hat{\beta}_1, \hat{\beta}_2\} \hat{u}_2^* \otimes \hat{v}_2^* \otimes \hat{w}_2^*$ with $\hat{\beta}_1, \hat{\beta}_2$ the estimated SNRs from step 4 of Algorithm 2.

Figure 6 depicts the performances of the standard orthogonalized deflation ($\gamma = 1$) and our proposed RTT-improved version, while varying the signal correlation parameter α . As theoretically anticipated, the RTT-improved algorithm recovers successively the signal components in the more challenging correlated setting (e.g., $\alpha \geq 0.3$).

4. Conclusion and Future Work

We have showcased a concrete example where random tensor theory allows us to understand and even improve signal recovery from low-rank asymmetric spiked random tensors. To the best of our knowledge, this is the first time where an asymptotic characterization of the considered deflation method is carried out. We highlight that our methodology can be straightforwardly generalized to higher order and higher (low) rank tensors in the same vein as (Seddik et al., 2021), which studied order- d and rank-one spiked tensor models. Such generalization will require more analytical computations and will result in more complicated systems of equations. Hence, for the sake of clarity, we limited our analysis to the simpler order-three and rank-two model.

Our approach has still many limitations and raises various open questions which we discuss as follows: (i) Our main results rely on Assumptions 3.1 and 3.5 which basically suppose the almost convergence of the singular values and alignments of

interest. Similar Assumptions were made and discussed in (Goulart et al., 2021; Seddik et al., 2021) which also relied on a RMT approach. A formal proof of these statements is still required and would make our analysis more complete. (ii) The second point concerns the existence and uniqueness of the solutions of the involved systems of equations. (iii) The third point concerns a proof of consistency of the underlying model parameters estimation. Specifically, proving a central limit theorem about the convergence of our estimates to the true parameters and the related conditions. We do not address these questions in our present analysis and we defer them to a future study.

Nevertheless, our actual results pave already a new path towards the analysis and improvement of more sophisticated tensor methods and models, by means of random tensor theory, thereby impacting tensor-based machine learning methods and many other applications which rely on tensors.

Code and Reproducibility: A Github repository will be provided for the reproducibility of our simulations and results, with an implementation of Algorithm 2.

References

- Anandkumar, A., Ge, R., Hsu, D., Kakade, S. M., and Telgarsky, M. Tensor decompositions for learning latent variable models. *Journal of machine learning research*, 15:2773–2832, 2014.
- Auddy, A. and Yuan, M. On estimating rank-one spiked tensors in the presence of heavy tailed errors. *IEEE Transactions on Information Theory*, 2022.
- Ben Arous, G., Huang, D. Z., and Huang, J. Long random matrices and tensor unfolding. *arXiv preprint arXiv:2110.10210*, 2021.
- Benaych-Georges, F., Guionnet, A., and Maida, M. Fluctuations of the extreme eigenvalues of finite rank deformations of random matrices. *Electronic Journal of Probability*, 16:1621–1662, 2011.
- Chen, W.-K., Handschy, M., and Lerman, G. Phase transition in random tensors with multiple independent spikes. *The Annals of Applied Probability*, 31(4):1868–1913, 2021.
- da Silva, A. P., Comon, P., and de Almeida, A. L. An iterative deflation algorithm for exact cp tensor decomposition. In *2015 IEEE International Conference on Acoustics, Speech and Signal Processing (ICASSP)*, pp. 3961–3965. IEEE, 2015a.
- da Silva, A. P., Comon, P., and de Almeida, A. L. F. Rank-1 tensor approximation methods and application to deflation. *arXiv preprint arXiv:1508.05273*, 2015b.
- Fawzi, A., Balog, M., Huang, A., Hubert, T., Romera-Paredes, B., Barekatain, M., Novikov, A., Ruiz, F. J., Schrittwieser, J., Swirszcz, G., et al. Discovering faster matrix multiplication algorithms with reinforcement learning. *Nature*, 610(7930):47–53, 2022.
- Goulart, J. H. d. M., Couillet, R., and Comon, P. A random matrix perspective on random tensors. *arXiv preprint arXiv:2108.00774*, 2021.
- Hachem, W., Loubaton, P., and Najim, J. Deterministic equivalents for certain functionals of large random matrices. *The Annals of Applied Probability*, 17(3):875–930, 2007.
- Hillar, C. J. and Lim, L.-H. Most tensor problems are NP-hard. *Journal of the ACM (JACM)*, 60(6):1–39, 2013.
- Huang, J., Huang, D. Z., Yang, Q., and Cheng, G. Power iteration for tensor pca. *Journal of Machine Learning Research*, 23(128):1–47, 2022.
- Jagannath, A., Lopatto, P., and Miolane, L. Statistical thresholds for tensor PCA. *The Annals of Applied Probability*, 30(4):1910–1933, 2020.
- Lesieur, T., Miolane, L., Lelarge, M., Krzakala, F., and Zdeborová, L. Statistical and computational phase transitions in spiked tensor estimation. In *2017 IEEE International Symposium on Information Theory (ISIT)*, pp. 511–515. IEEE, 2017.

- Lim, L.-H. Singular values and eigenvalues of tensors: a variational approach. In *Proc. IEEE International Workshop on Computational Advances in Multi-Sensor Adaptive Processing (CAMSAP)*, pp. 129–132, 2005.
- Louart, C. and Couillet, R. Concentration of measure and large random matrices with an application to sample covariance matrices. *arXiv preprint arXiv:1805.08295*, 2018.
- Mackey, L. Deflation methods for sparse pca. *Advances in neural information processing systems*, 21, 2008.
- Perry, A., Wein, A. S., and Bandeira, A. S. Statistical limits of spiked tensor models. In *Annales de l’Institut Henri Poincaré, Probabilités et Statistiques*, volume 56, pp. 230–264. Institut Henri Poincaré, 2020.
- Rabanser, S., Shchur, O., and Günnemann, S. Introduction to tensor decompositions and their applications in machine learning. *arXiv preprint arXiv:1711.10781*, 2017.
- Richard, E. and Montanari, A. A statistical model for tensor PCA. *Advances in neural information processing systems*, 27, 2014.
- Seddik, M. E. A., Guillaud, M., and Couillet, R. When random tensors meet random matrices. *arXiv preprint arXiv:2112.12348*, 2021.
- Seddik, M. E. A., Guillaud, M., and Decurninge, A. On the accuracy of hotelling-type tensor deflation: A random tensor analysis. *arXiv preprint arXiv:2211.09004*, 2022.
- Sidiropoulos, N. D., De Lathauwer, L., Fu, X., Huang, K., Papalexakis, E. E., and Faloutsos, C. Tensor decomposition for signal processing and machine learning. *IEEE Transactions on Signal Processing*, 65(13):3551–3582, 2017.
- Silverstein, J. W. and Bai, Z. On the empirical distribution of eigenvalues of a class of large dimensional random matrices. *Journal of Multivariate analysis*, 54(2):175–192, 1995.
- Stegeman, A. and Comon, P. Subtracting a best rank-1 approximation may increase tensor rank. *Linear Algebra and its Applications*, 433(7):1276–1300, 2010.
- Stein, C. M. Estimation of the mean of a multivariate normal distribution. *The annals of Statistics*, pp. 1135–1151, 1981.
- Strassen, V. Rank and optimal computation of generic tensors. *Linear algebra and its applications*, 52:645–685, 1983.
- Tao, T. *Topics in random matrix theory*, volume 132. American Mathematical Soc., 2012.
- Van Der Vaart, A. W. and Wellner, J. A. Weak convergence. In *Weak convergence and empirical processes*, pp. 16–28. Springer, 1996.
- Wang, Z., Lee, J., and Lei, Q. Reconstructing training data from model gradient, provably. *arXiv preprint arXiv:2212.03714*, 2022.
- Zare, A., Ozdemir, A., Iwen, M. A., and Aviyente, S. Extension of pca to higher order data structures: An introduction to tensors, tensor decompositions, and tensor pca. *Proceedings of the IEEE*, 106(8):1341–1358, 2018.

5. Additional Simulations

5.1. Simulated and Asymptotic Alignments at Second Deflation Step

Figure 7 depicts the simulated and asymptotic singular value and alignments of the second deflation step as described in Section 3.2.2. Since Theorem 3.7 requires Assumption 3.5, the system of equations in (14) may have many solutions in general, but when initializing it with the simulated values of λ_2 and alignments, we obtain consistent characterization of their asymptotic counterparts. As we discussed in the conclusion, the existence and uniqueness of the solutions of (14) is left for a future study.

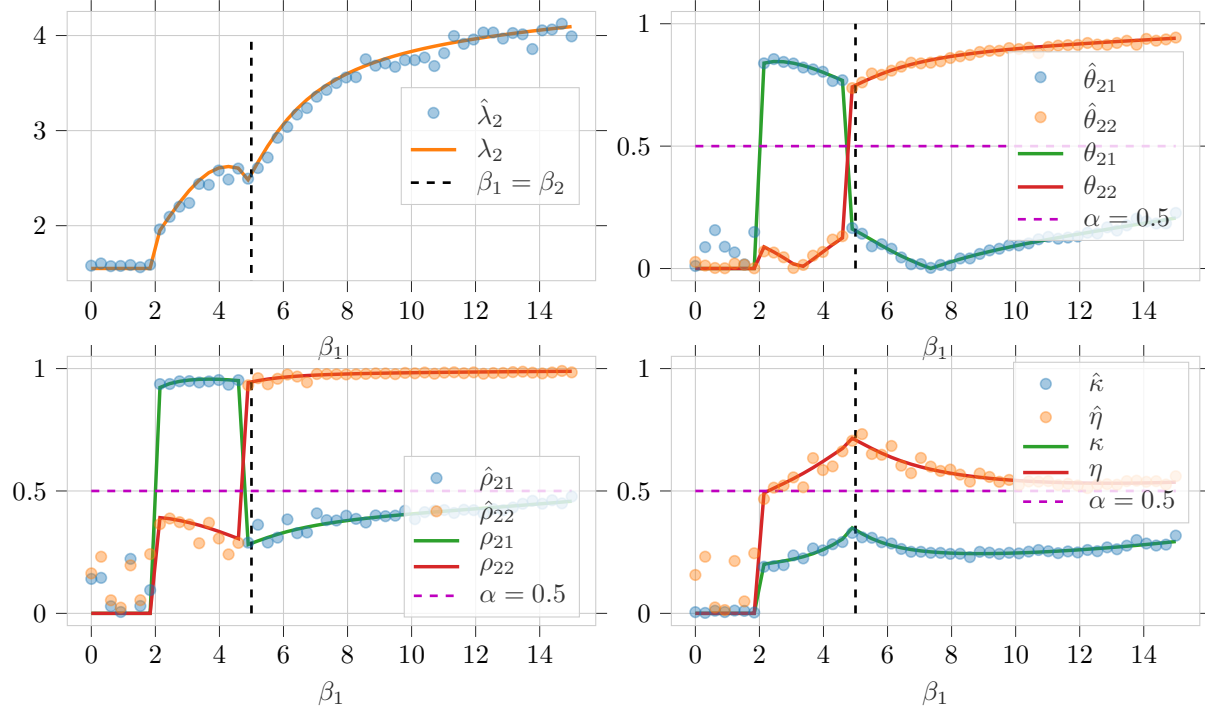


Figure 7. Simulated versus asymptotic singular value and alignments corresponding to the second deflation step as per Theorem 3.7. We considered $\beta_1 = 5$, $\alpha = 0.5$, $p = 100$, $\gamma = 0.8$ and varying $\beta_1 \in [0, 15]$. The system of equations in (14) is solved numerically and initialized with the simulated singular value and alignments (dotted curves) from one realization of \mathcal{T}_1 .

5.2. More on Model Parameters Estimation

In this section, we provide more discussions about the model parameters estimation described in Section 3.2.3. An import aspect about such estimation, is to prove its consistency. Namely, demonstrating a CLT result which shows the concentration of $\hat{\beta}$ around the true β as well as for $\hat{\rho}$. We currently support this statement through simulations as depicted in Figures 9 and 10. Note however that, given the concentration of $\hat{\lambda}$, we believe that such consistency can be ensured with additional assumptions on the function ψ in (16) and in particular the existence and uniqueness of solution to the equation $\psi(\cdot, \hat{\lambda}, \cdot) = 0$.

$$\psi : (\beta, \lambda, \rho) \mapsto \begin{pmatrix} f_r(\lambda_1) - \sum_{i=1}^2 \beta_i \rho_{1i}^3 \\ h_r(\lambda_1) \rho_{11} - \sum_{i=1}^2 \beta_i \alpha_{i1} \rho_{1i}^2 \\ h_r(\lambda_1) \rho_{12} - \sum_{i=1}^2 \beta_i \alpha_{i2} \rho_{1i}^2 \\ f_r(\lambda_2) - \sum_{i=1}^2 \beta_i \theta_{2i} \rho_{2i}^2 \\ h_r(\lambda_2) \theta_{21} - \frac{\eta^2}{3} r(\lambda_1) \rho_{11} - \sum_{i=1}^2 \beta_i \alpha_{i1} \rho_{2i}^2 + \rho_{11} \sum_{i=1}^2 \beta_i \rho_{1i} \rho_{2i}^2 \\ h_r(\lambda_2) \theta_{22} - \frac{\eta^2}{3} r(\lambda_1) \rho_{12} - \sum_{i=1}^2 \beta_i \alpha_{i2} \rho_{2i}^2 + \rho_{12} \sum_{i=1}^2 \beta_i \rho_{1i} \rho_{2i}^2 \\ h_r(\lambda_2) \rho_{21} - \sum_{i=1}^2 \beta_i \theta_{2i} \rho_{2i} \alpha_{i1} \\ h_r(\lambda_2) \rho_{22} - \sum_{i=1}^2 \beta_i \theta_{2i} \rho_{2i} \alpha_{i2} \\ [\lambda_2 + \frac{2}{3} r(\lambda_2)] \eta - \sum_{i=1}^2 \beta_i \theta_{2i} \rho_{1i} \rho_{2i} \end{pmatrix}. \quad (16)$$

6. Some Key Lemmas

In this section, we recall some key lemmas that are at the heart of our analysis.

Lemma 6.1 (Woodbury matrix identity). *Let $A \in \mathbb{R}^{n \times n}$, $B \in \mathbb{R}^{r \times r}$, $U \in \mathbb{R}^{n \times r}$ and $V \in \mathbb{R}^{r \times n}$, we have*

$$(A + UVB)^{-1} = A^{-1} - A^{-1}U(B^{-1} + VA^{-1}U)^{-1}VA^{-1}$$

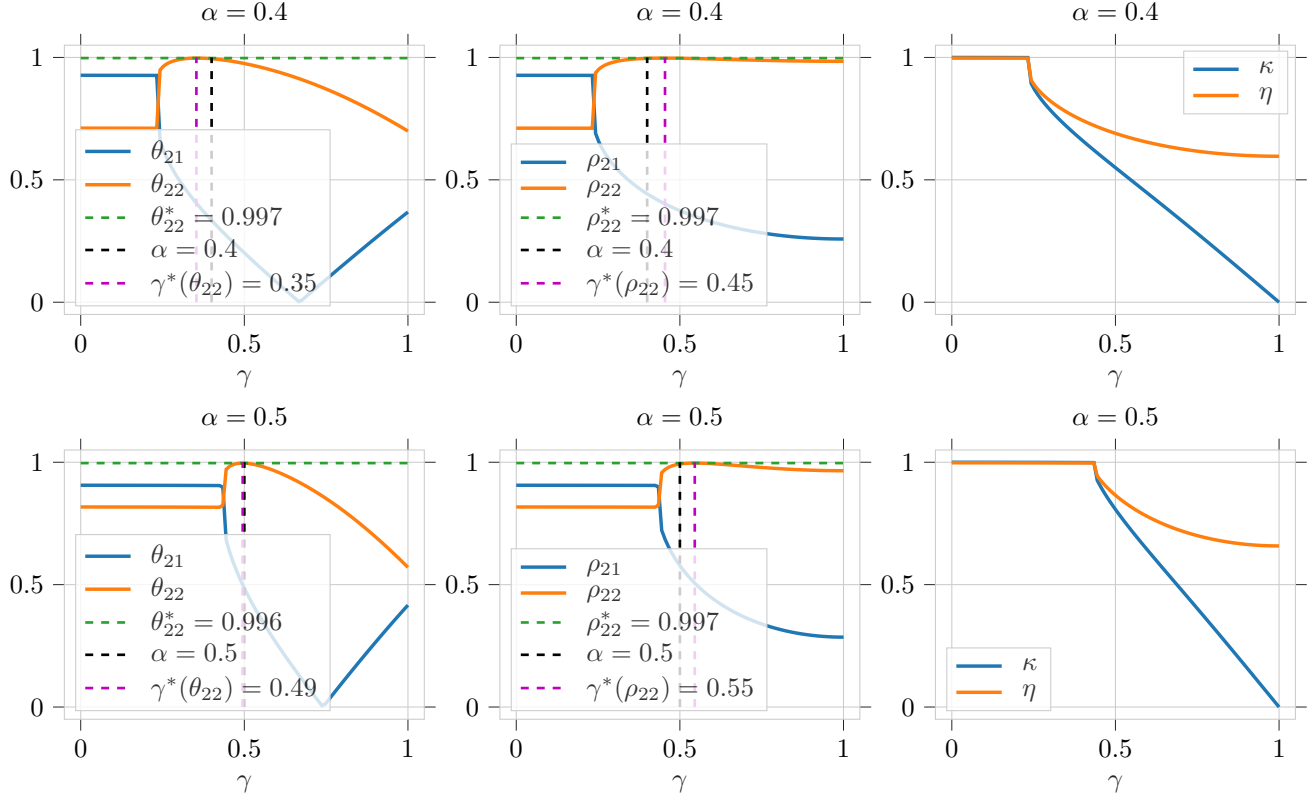


Figure 8. Asymptotic alignments of the second deflation step in terms of γ and α . We considered $\beta_1 = 10$ and $\beta_2 = 8$.

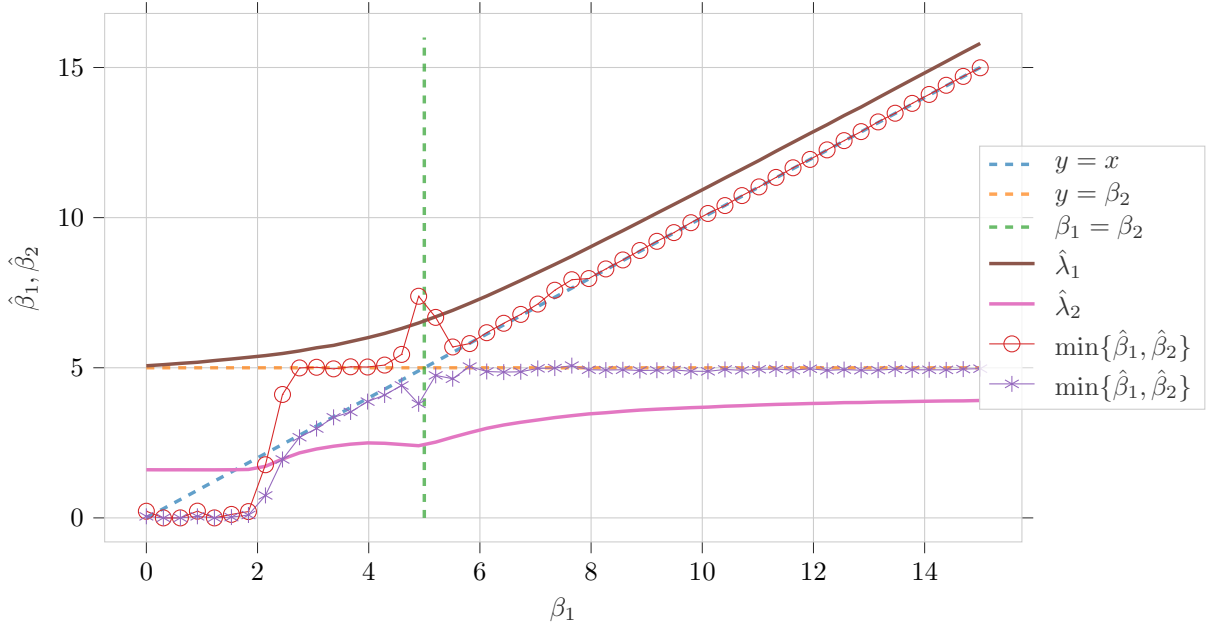


Figure 9. Estimation of the underlying SNRs β_1 and β_2 as described in Section 3.2.3. We considered $\beta_2 = 5$, $\alpha = 0.5$, $p = 150$ and $\gamma = 1$ while varying β_2 . The parameters are estimated only from the singular values $\hat{\lambda}_1$, $\hat{\lambda}_2$ and the alignment between the singular vectors $\hat{\eta} = \langle \hat{v}_1, \hat{v}_2 \rangle$, computed via tensor power iteration. The curves are averaged over 100 realizations of \mathcal{T}_1 .

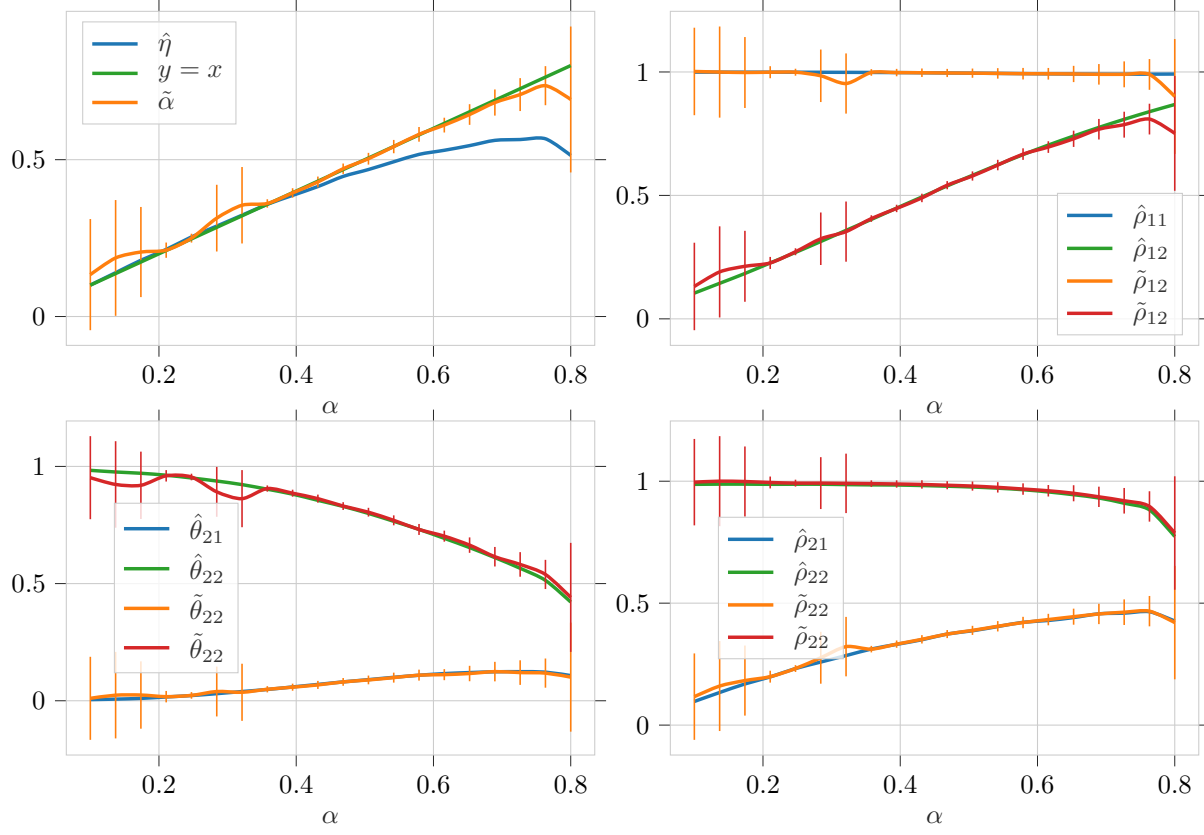


Figure 10. Estimation of the alignments as described in Section 3.2.3 from one realization of the random tensor \mathcal{T}_1 . We considered $\beta_1 = 15$, $\beta_2 = 5$, $\gamma = 1$, $p = 100$ while varying α . The curves are averaged over 100 realizations of \mathcal{T}_1 . The hats correspond to simulations while tildes correspond to the estimated alignments as per Section 3.2.3.

The following perturbation lemma is widely used in RMT. Basically, it states that the normalized trace operator is invariant through low-rank perturbations in high dimension. The notation $a = O_n(b_n)$ means that a is of order $O(b_n)$ as $n \rightarrow \infty$.

Lemma 6.2 (Perturbation lemma (Silverstein & Bai, 1995)). *Let $M \in \mathbb{R}^{n \times n}$ and $P \in \mathbb{R}^{n \times n}$ such that $\|M\| = O_n(1)$, $\|P\| = O_n(1)$ and $\text{rank}(P) = O_n(1)$. For all $z \in \mathbb{C} \setminus \text{Sp}(M + P)$, we have*

$$\frac{1}{n} \text{tr}(M + P - zI_n)^{-1} = \frac{1}{n} \text{tr}(M - zI_n)^{-1} + O_n(n^{-1})$$

Proof. Simple consequence of the Woodbury identity from Lemma 6.1 applied to the matrix $M + P$. \square

Our analysis will particularly rely on computing expectations which we drive through the classical Stein's Lemma.

Lemma 6.3 (Stein's Lemma (Stein, 1981)). *Let $W \sim \mathcal{N}(0, \sigma^2)$ and f some continuously differentiable function having at most polynomial growth, then*

$$\mathbb{E}[W f(W)] = \sigma^2 \mathbb{E}[f'(W)]$$

when the above expectations exist.

7. Proofs of the main results

We recall our considered spiked tensor model as follows

$$\mathcal{T}_1 = \mathcal{S} + \frac{1}{\sqrt{n}} \mathcal{W} \in \mathbb{R}^{p \times p \times p} \quad \text{with} \quad \mathcal{S} = \sum_{i=1}^2 \beta_i x_i \otimes y_i \otimes z_i \quad (17)$$

where $\|x_i\| = \|y_i\| = \|z_i\| = 1$, $\beta_i \geq 0$, $n = 3p$ and $W_{ijk} \sim \mathcal{N}(0, 1)$. In the remainder, if some quantity expresses as $a(n) = \sum_{i=1}^r b_i(n)$, the notation $a(n) \simeq b_j(n)$ means that $b_j(n)$ is the only contributing term in the expression of $a(n)$ as n goes to infinity.

7.1. First deflation step

The singular vectors u_1, v_1 and w_1 of \mathcal{T}_1 corresponding to its largest singular value λ_1 satisfy

$$\mathcal{T}_1(\cdot, v_1, w_1) = \lambda_1 u_1, \quad \mathcal{T}_1(u_1, \cdot, w_1) = \lambda_1 v_1, \quad \mathcal{T}_1(u_1, v_1, \cdot) = \lambda_1 w_1 \quad (18)$$

In the remainder, we will need to compute the derivatives of the singular vectors u_1, v_1 and w_1 w.r.t. the entries of the noise tensor \mathcal{W} . From (Seddik et al., 2021, Appendix B.1), we have

$$\begin{pmatrix} \frac{\partial u_1}{\partial W_{ijk}} \\ \frac{\partial v_1}{\partial W_{ijk}} \\ \frac{\partial w_1}{\partial W_{ijk}} \end{pmatrix} = -\frac{1}{\sqrt{n}} \left(\begin{pmatrix} 0 & \mathcal{T}_1(w_1) & \mathcal{T}_1(v_1) \\ \mathcal{T}_1(w_1)^\top & 0 & \mathcal{T}_1(u_1) \\ \mathcal{T}_1(v_1)^\top & \mathcal{T}_1(u_1)^\top & 0 \end{pmatrix} - \lambda_1 \mathbf{I}_n \right)^{-1} \begin{pmatrix} v_{1j} w_{1k} (e_i - u_{1i} u_1) \\ u_{1i} w_{1k} (e_j - v_{1j} v_1) \\ u_{1i} v_{1j} (e_k - w_{1k} w_1) \end{pmatrix} \quad (19)$$

which results from deriving the identities in (18) w.r.t. the entry W_{ijk} of the noise tensor \mathcal{W} . In particular, as demonstrated in (Seddik et al., 2021), the only contributing terms in the quantities we will compute later on will depend only on traces of the resolvent matrix appearing in (19).

7.1.1. LIMITING STIELTJES TRANSFORM

Since the tensor \mathcal{T}_1 is a low-rank perturbation of a random tensor \mathcal{W} , by Lemma 6.2, the normalized trace of the resolvent in (19) is asymptotically equal to the normalized trace of the resolvent of the following random matrix

$$\mathbf{N} = \frac{1}{\sqrt{n}} \begin{pmatrix} 0 & \mathcal{W}(w_1) & \mathcal{W}(v_1) \\ \mathcal{W}(w_1)^\top & 0 & \mathcal{W}(u_1) \\ \mathcal{W}(v_1)^\top & \mathcal{W}(u_1)^\top & 0 \end{pmatrix} \quad (20)$$

Let $R(z) = (\mathbf{N} - z \mathbf{I}_n)^{-1}$ be the corresponding resolvent. We denote the different sub-blocks of $R(z)$ as

$$R(z) = \begin{pmatrix} R^{11}(z) & R^{12}(z) & R^{13}(z) \\ R^{12}(z)^\top & R^{22}(z) & R^{23}(z) \\ R^{13}(z)^\top & R^{23}(z)^\top & R^{33}(z) \end{pmatrix} \quad (21)$$

It has been shown in (Seddik et al., 2021, Appendix B.2) that

$$\frac{1}{n} \text{tr} R^{ii}(z) \xrightarrow{n \rightarrow \infty} r_i(z) = \frac{r(z)}{3} \quad \text{and} \quad \frac{1}{n} \text{tr} R(z) \xrightarrow{n \rightarrow \infty} r(z) \quad (22)$$

with

$$r(z) = \frac{3}{4} \left(-z + \sqrt{z^2 - \frac{8}{3}} \right) \quad (23)$$

7.1.2. ESTIMATION OF THE SINGULAR VALUE

Estimation of λ_1 : From the identities in (18), we have

$$\lambda_1 = \mathcal{T}_1(u_1, v_1, w_1) = \mathcal{S}(u_1, v_1, w_1) + \frac{1}{\sqrt{n}} \mathcal{W}(u_1, v_1, w_1)$$

and

$$\begin{aligned} \frac{1}{\sqrt{n}} \mathbb{E}[\mathcal{W}(u_1, v_1, w_1)] &= \frac{1}{\sqrt{n}} \sum_{ijk} \mathbb{E}[u_{1i} v_{1j} w_{1k} W_{ijk}] \\ &= \frac{1}{\sqrt{n}} \sum_{ijk} \mathbb{E} \left[\frac{\partial u_{1i}}{\partial W_{ijk}} v_{1j} w_{1k} \right] + \mathbb{E} \left[u_{1i} \frac{\partial v_{1j}}{\partial W_{ijk}} w_{1k} \right] + \mathbb{E} \left[u_{1i} v_{1j} \frac{\partial w_{1k}}{\partial W_{ijk}} \right] \end{aligned}$$

where the last equality is derived from Stein's Lemma and the involved derivatives express as

$$\frac{\partial u_{1i}}{\partial W_{ijk}} \simeq \frac{-1}{\sqrt{n}} v_{1j} w_{1k} R_{ii}^{11}(\lambda_1), \quad \frac{\partial v_{1j}}{\partial W_{ijk}} \simeq \frac{-1}{\sqrt{n}} u_{1i} w_{1k} R_{jj}^{22}(\lambda_1), \quad \frac{\partial w_{1k}}{\partial W_{ijk}} \simeq \frac{-1}{\sqrt{n}} u_{1i} v_{1j} R_{kk}^{33}(\lambda_1)$$

Substituting in the above sum, we get

$$\begin{aligned} \frac{1}{\sqrt{n}} \mathbb{E}[\mathcal{W}(u_1, v_1, w_1)] &\simeq -\frac{1}{n} \sum_{ijk} \mathbb{E}[v_{1j}^2 w_{1k}^2 R_{ii}^{11}(\lambda_1)] - \frac{1}{n} \sum_{ijk} \mathbb{E}[u_{1i}^2 w_{1k}^2 R_{jj}^{22}(\lambda_1)] - \frac{1}{n} \sum_{ijk} \mathbb{E}[u_{1i}^2 v_{1j}^2 R_{kk}^{33}(\lambda_1)] \\ &= -\mathbb{E}\left[\frac{1}{n} \text{tr} R^{11}(\lambda_1)\right] - \mathbb{E}\left[\frac{1}{n} \text{tr} R^{22}(\lambda_1)\right] - \mathbb{E}\left[\frac{1}{n} \text{tr} R^{33}(\lambda_1)\right] \\ &\xrightarrow{n \rightarrow \infty} -(r_1(\lambda_1) + r_2(\lambda_1) + r_3(\lambda_1)) = -r(\lambda_1) \end{aligned}$$

Therefore, we have

$$\lambda_1 + r(\lambda_1) = \mathcal{S}(u_1, v_1, w_1) \quad (24)$$

7.1.3. ESTIMATION OF THE ALIGNMENTS

Estimation of $\langle u_1, x_s \rangle$: Again from the first identity in (18), we have

$$\lambda_1 \langle u_1, x_s \rangle = \mathcal{T}_1(x_s, v_1, w_1) = \mathcal{S}(x_s, v_1, w_1) + \frac{1}{\sqrt{n}} \mathcal{W}(x_s, v_1, w_1)$$

And we have

$$\begin{aligned} \frac{1}{\sqrt{n}} \mathbb{E}[\mathcal{W}(x_s, v_1, w_1)] &= \frac{1}{\sqrt{n}} \sum_{ijk} \mathbb{E}[x_{si} v_{1j} w_{1k} W_{ijk}] \\ &= \frac{1}{\sqrt{n}} \sum_{ijk} \mathbb{E}\left[x_{si} \frac{\partial v_{1j}}{\partial W_{ijk}} w_{1k}\right] + \frac{1}{\sqrt{n}} \sum_{ijk} \mathbb{E}\left[x_{si} v_{1j} \frac{\partial w_{1k}}{\partial W_{ijk}}\right] \\ &\simeq -\frac{1}{n} \sum_{ijk} \mathbb{E}[x_{si} u_{1i} w_{1k}^2 R_{jj}^{22}(\lambda_1)] - \frac{1}{n} \sum_{ijk} \mathbb{E}[x_{si} u_{1i} v_{1j}^2 R_{kk}^{33}(\lambda_1)] \\ &= -\mathbb{E}\left[\langle x_s, u_1 \rangle \frac{1}{n} \text{tr} R^{22}(\lambda_1)\right] - \mathbb{E}\left[\langle x_s, u_1 \rangle \frac{1}{n} \text{tr} R^{33}(\lambda_1)\right] \\ &\xrightarrow{n \rightarrow \infty} -(r_2(\lambda_1) + r_3(\lambda_1)) \langle x_s, u_1 \rangle = -(r(\lambda_1) - r_1(\lambda_1)) \langle x_s, u_1 \rangle \end{aligned}$$

Therefore, we have

$$(\lambda_1 + r(\lambda_1) - r_1(\lambda_1)) \langle x_s, u_1 \rangle = \mathcal{S}(x_s, v_1, w_1) \quad (25)$$

Similarly, we get

$$\begin{aligned} (\lambda_1 + r(\lambda_1) - r_2(\lambda_1)) \langle y_s, v_1 \rangle &= \mathcal{S}(u_1, y_s, w_1) \\ (\lambda_1 + r(\lambda_1) - r_3(\lambda_1)) \langle z_s, w_1 \rangle &= \mathcal{S}(u_1, v_1, z_s) \end{aligned} \quad (26)$$

Finally, with our assumption in (3) and since \mathcal{T}_1 is cubic, the above equations reduce to the following system of equations describing the first deflation step

$$\boxed{\begin{cases} f_r(\lambda_1) = \sum_{i=1}^2 \beta_i \rho_{1i}^3 \\ h_r(\lambda_1) \rho_{1j} = \sum_{i=1}^2 \beta_i \langle x_i, x_j \rangle \rho_{1i}^2 \quad \text{for } j \in [2] \end{cases}} \quad (27)$$

where we denoted $f_r(z) = z + r(z)$ and $h_r(z) = z + \frac{2}{3}r(z) = -\frac{1}{r(z)}$.

7.2. Second deflation step

Given u_1 from the first deflation step, we consider now the following random tensor

$$\mathcal{T}_2 = \mathcal{T}_1 \times_1 (\mathbf{I}_N - \gamma u_1 u_1^\top) = \mathcal{T}_1 - \gamma u_1 \otimes \mathcal{T}_1(u_1, \cdot, \cdot) \quad (28)$$

Again the singular vectors of \mathcal{T}_2 satisfy

$$\mathcal{T}_2(\cdot, v_2, w_2) = \lambda_2 u_2, \quad \mathcal{T}_2(u_2, \cdot, w_2) = \lambda_2 v_2, \quad \mathcal{T}_2(u_2, v_2, \cdot) = \lambda_2 w_2 \quad (29)$$

and we also have

$$\begin{pmatrix} \frac{\partial u_2}{\partial W_{ijk}} \\ \frac{\partial v_2}{\partial W_{ijk}} \\ \frac{\partial w_2}{\partial W_{ijk}} \end{pmatrix} = -\frac{1}{\sqrt{n}} \left(\begin{pmatrix} 0 & \mathcal{T}_2(w_2) & \mathcal{T}_2(v_2) \\ \mathcal{T}_2(w_2)^\top & 0 & \mathcal{T}_2(u_2) \\ \mathcal{T}_2(v_2)^\top & \mathcal{T}_2(u_2)^\top & 0 \end{pmatrix} - \lambda_2 \mathbf{I}_n \right)^{-1} \begin{pmatrix} v_2 w_2 (e_i - u_2 u_2^\top) \\ u_2 w_2 (e_j - v_2 v_2^\top) \\ u_2 v_2 (e_k - w_2 w_2^\top) \end{pmatrix} \quad (30)$$

7.2.1. STIELTJES TRANSFORM

Again, since \mathcal{T}_1 is a low-rank perturbation of a random tensor \mathcal{W} , it is easily noticed that

$$\begin{pmatrix} 0 & \mathcal{T}_2(w_2) & \mathcal{T}_2(v_2) \\ \mathcal{T}_2(w_2)^\top & 0 & \mathcal{T}_2(u_2) \\ \mathcal{T}_2(v_2)^\top & \mathcal{T}_2(u_2)^\top & 0 \end{pmatrix} = \mathbf{M} + \mathbf{P}$$

where \mathbf{P} is some low-rank matrix and \mathbf{M} is a random matrix given by

$$\mathbf{M} = \frac{1}{\sqrt{n}} \begin{pmatrix} 0 & \mathcal{W}(w_2) & \mathcal{W}(v_2) \\ \mathcal{W}(w_2)^\top & 0 & \mathcal{W}(u_2) - \gamma \langle u_1, u_2 \rangle \mathcal{W}(u_1)^\top \\ \mathcal{W}(v_2)^\top & \mathcal{W}(u_2)^\top - \gamma \langle u_1, u_2 \rangle \mathcal{W}(u_1)^\top & 0 \end{pmatrix} \quad (31)$$

Therefore, by Lemma 6.2, the limiting Stieltjes transform corresponding to the analysis of the second deflation step can be computed through the resolvent $Q(z) = (\mathbf{M} - z\mathbf{I}_n)^{-1}$ of the random matrix \mathbf{M} and we denote $\kappa = \langle u_1, u_2 \rangle$. We denote the different sub-blocks of $Q(z)$ as

$$Q(z) = \begin{pmatrix} Q^{11}(z) & Q^{12}(z) & Q^{13}(z) \\ Q^{12}(z)^\top & Q^{22}(z) & Q^{23}(z) \\ Q^{13}(z)^\top & Q^{23}(z)^\top & Q^{33}(z) \end{pmatrix} \quad (32)$$

Denote

$$\frac{1}{n} \text{tr} Q^{ii}(z) \xrightarrow{n \rightarrow \infty} q_i(z) \quad \text{and} \quad \frac{1}{n} \text{tr} Q(z) \xrightarrow{n \rightarrow \infty} q(z) \quad (33)$$

Estimation of $\frac{1}{n} \text{tr} Q^{11}(z)$: From the identity $\mathbf{M}Q(z) - zQ(z) = \mathbf{I}_n$, we have

$$\frac{1}{\sqrt{n}} [\mathcal{W}(w_2)(Q^{12})^\top]_{ii} + \frac{1}{\sqrt{n}} [\mathcal{W}(v_2)(Q^{13})^\top]_{ii} - zQ_{ii}^{11} = 1$$

Therefore

$$\frac{1}{n\sqrt{n}} \sum_{ijk} \mathbb{E} [w_{2k} W_{ijk} Q_{ij}^{12}] + \frac{1}{n\sqrt{n}} \sum_{ijk} \mathbb{E} [v_{2j} W_{ijk} Q_{ik}^{13}] - \frac{z}{n} \text{tr} Q^{11}(z) = \frac{1}{3}$$

where

$$\bullet \quad \frac{1}{n\sqrt{n}} \sum_{ijk} \mathbb{E} [w_{2k} W_{ijk} Q_{ij}^{12}] \simeq \frac{1}{n\sqrt{n}} \sum_{ijk} \mathbb{E} \left[w_{2k} \frac{\partial Q_{ij}^{12}}{\partial W_{ijk}} \right]$$

From (Seddik et al., 2021), we have $\frac{\partial Q_{ij}^{12}}{\partial W_{ijk}} \simeq -\frac{1}{\sqrt{n}} w_{2k} Q_{ii}^{11} Q_{jj}^{22}$, hence

$$\frac{1}{n\sqrt{n}} \sum_{ijk} \mathbb{E} [w_{2k} W_{ijk} Q_{ij}^{12}] \simeq -\frac{1}{n^2} \sum_{ijk} \mathbb{E} [w_{2k}^2 Q_{ii}^{11} Q_{jj}^{22}] = -\mathbb{E} \left[\frac{1}{n} \text{tr} Q^{11} \frac{1}{n} \text{tr} Q^{22} \right] \xrightarrow{n \rightarrow \infty} -q_1(z) q_2(z)$$

Similarly, we have

$$\bullet \quad \frac{1}{n\sqrt{n}} \sum_{ijk} \mathbb{E} [v_{2j} W_{ijk} Q_{ik}^{13}] \xrightarrow{n \rightarrow \infty} -q_1(z) q_3(z)$$

Therefore, $q_1(z) = \lim_{n \rightarrow \infty} \frac{1}{n} \text{tr} Q^{11}(z)$ satisfies the equation

$$[q_2(z) + q_3(z) + z] q_1(z) + \frac{1}{3} = 0 \quad (34)$$

Estimation of $\frac{1}{n} \text{tr} Q^{22}(z)$: We have

$$\frac{1}{\sqrt{n}} [\mathcal{W}(w_2)^\top Q^{12}]_{jj} + \frac{1}{\sqrt{n}} [(\mathcal{W}(u_2) - \gamma \kappa \mathcal{W}(u_1)) (Q^{23})^\top]_{jj} - z Q_{jj}^{22} = 1$$

Hence

$$\frac{1}{n\sqrt{n}} \sum_{ijk} \mathbb{E} [w_{2k} W_{ijk} Q_{ij}^{12}] + \frac{1}{n\sqrt{n}} \sum_{ijk} \mathbb{E} [u_{2i} W_{ijk} Q_{jk}^{23}] - \frac{\gamma \kappa}{n\sqrt{n}} \sum_{ijk} \mathbb{E} [u_{1i} W_{ijk} Q_{jk}^{23}] - \frac{z}{n} \text{tr} Q^{22} = \frac{1}{3}$$

where

$$\begin{aligned} \bullet \quad & \frac{1}{n\sqrt{n}} \sum_{ijk} \mathbb{E} [w_{2k} W_{ijk} Q_{ij}^{12}] \simeq \frac{1}{n\sqrt{n}} \sum_{ijk} \mathbb{E} \left[w_{2k} \frac{\partial Q_{ij}^{12}}{\partial W_{ijk}} \right] = -\frac{1}{n^2} \sum_{ijk} \mathbb{E} [w_{2k}^2 Q_{ii}^{11} Q_{jj}^{22}] \xrightarrow{n \rightarrow \infty} -q_1(z) q_2(z) \\ \bullet \quad & \frac{1}{n\sqrt{n}} \sum_{ijk} \mathbb{E} [u_{2i} W_{ijk} Q_{jk}^{23}] \simeq \frac{1}{n\sqrt{n}} \sum_{ijk} \mathbb{E} \left[u_{2i} \frac{\partial Q_{jk}^{23}}{\partial W_{ijk}} \right] = -\frac{1}{n^2} \sum_{ijk} \mathbb{E} [(u_{2i}^2 - \gamma \kappa u_{1i} u_{2i}) Q_{jj}^{22} Q_{kk}^{33}] \xrightarrow{n \rightarrow \infty} (\gamma \kappa^2 - 1) q_2(z) q_3(z) \\ \bullet \quad & \frac{1}{n\sqrt{n}} \sum_{ijk} \mathbb{E} [u_{1i} W_{ijk} Q_{jk}^{23}] \simeq \frac{1}{n\sqrt{n}} \sum_{ijk} \mathbb{E} \left[u_{1i} \frac{\partial Q_{jk}^{23}}{\partial W_{ijk}} \right] = -\frac{1}{n^2} \sum_{ijk} \mathbb{E} [(u_{1i} u_{2i} - \gamma \kappa u_{1i}^2) Q_{jj}^{22} Q_{kk}^{33}] \xrightarrow{n \rightarrow \infty} \kappa(\gamma - 1) q_2(z) q_3(z) \end{aligned}$$

where we used the fact that $\frac{\partial Q_{jk}^{23}}{\partial W_{ijk}} \simeq -\frac{1}{\sqrt{n}} (u_{2i} - \gamma \kappa u_{1i}) Q_{jj}^{22} Q_{kk}^{33}$.

$$(q_1(z) + z - [\gamma \kappa^2 - 1 + \kappa(\gamma - 1)] q_3(z)) q_2(z) + \frac{1}{3} = 0 \quad (35)$$

Estimation of $\frac{1}{n} \text{tr} Q^{33}(z)$: From the identity $\mathbf{M}Q(z) - zQ(z) = \mathbf{I}_n$, we have

$$\frac{1}{\sqrt{n}} [\mathcal{W}(v_2)^\top Q^{13}]_{kk} + \frac{1}{\sqrt{n}} [(\mathcal{W}(u_2)^\top - \gamma \kappa \mathcal{W}(u_1)^\top) (Q^{23})]_{kk} - z Q_{kk}^{33} = 1$$

Hence

$$\frac{1}{n\sqrt{n}} \sum_{ijk} \mathbb{E} [v_{2j} W_{ijk} Q_{ik}^{13}] + \frac{1}{n\sqrt{n}} \sum_{ijk} \mathbb{E} [u_{2i} W_{ijk} Q_{jk}^{23}] - \gamma \kappa \frac{1}{n\sqrt{n}} \sum_{ijk} \mathbb{E} [u_{1i} W_{ijk} Q_{jk}^{23}] - \frac{z}{n} \text{tr} Q^{33}(z) = \frac{1}{3}$$

where

$$\frac{1}{n\sqrt{n}} \sum_{ijk} \mathbb{E} [v_{2j} W_{ijk} Q_{ik}^{13}] \simeq \frac{1}{n\sqrt{n}} \sum_{ijk} \mathbb{E} \left[v_{2j} \frac{\partial Q_{ik}^{13}}{\partial W_{ijk}} \right] = -\frac{1}{n^2} \sum_{ijk} \mathbb{E} [v_{2j}^2 Q_{ii}^{11} Q_{kk}^{33}] \xrightarrow{n \rightarrow \infty} -q_1(z) q_3(z)$$

$$\frac{1}{n\sqrt{n}} \sum_{ijk} \mathbb{E} [u_{2i} W_{ijk} Q_{jk}^{23}] \simeq \frac{1}{n\sqrt{n}} \sum_{ijk} \mathbb{E} \left[u_{2i} \frac{\partial Q_{jk}^{23}}{\partial W_{ijk}} \right] = -\frac{1}{n^2} \sum_{ijk} \mathbb{E} [(u_{2i}^2 - \gamma \kappa u_{1i} u_{2i}) Q_{jj}^{22} Q_{kk}^{33}] \xrightarrow{n \rightarrow \infty} (\gamma \kappa^2 - 1) q_2(z) q_3(z)$$

$$\frac{1}{n\sqrt{n}} \sum_{ijk} \mathbb{E} [u_{1i} W_{ijk} Q_{jk}^{23}] \simeq \frac{1}{n\sqrt{n}} \sum_{ijk} \mathbb{E} \left[u_{1i} \frac{\partial Q_{jk}^{23}}{\partial W_{ijk}} \right] = -\frac{1}{n^2} \sum_{ijk} \mathbb{E} [(u_{1i} u_{2i} - \gamma \kappa u_{1i}^2) Q_{jj}^{22} Q_{kk}^{33}] \xrightarrow{n \rightarrow \infty} \kappa(\gamma - 1) q_2(z) q_3(z)$$

with again $\frac{\partial Q_{jk}^{23}}{\partial W_{ijk}} \simeq -\frac{1}{\sqrt{n}}(u_{2i} - \gamma \kappa u_{1i}) Q_{jj}^{22} Q_{kk}^{33}$.

$$(q_1(z) + z - [\gamma \kappa^2 - 1 + \kappa(\gamma - 1)] q_2(z)) q_3(z) + \frac{1}{3} = 0 \quad (36)$$

Therefore, we have

$$\begin{cases} [q_2(z) + q_3(z) + z] q_1(z) + \frac{1}{3} = 0 \\ (q_1(z) + z - [\gamma \kappa^2 - 1 + \kappa(\gamma - 1)] q_3(z)) q_2(z) + \frac{1}{3} = 0 \\ (q_1(z) + z - [\gamma \kappa^2 - 1 + \kappa(\gamma - 1)] q_2(z)) q_3(z) + \frac{1}{3} = 0 \\ q(z) = \sum_{i=1}^3 q_i(z) \end{cases} \quad (37)$$

Moreover, by symmetry in (3) and since \mathcal{T}_1 is cubic, we have $b(z) = q_2(z) = q_3(z)$ and we denote $a(z) = q_1(z)$ and $\tau = \gamma \kappa^2 - 1 + \kappa(\gamma - 1)$. Hence,

$$\boxed{\begin{cases} [2b(z) + z] a(z) + \frac{1}{3} = 0 \\ (a(z) + z - \tau b(z)) b(z) + \frac{1}{3} = 0 \end{cases}} \quad (38)$$

Moreover, $q(z) = a(z) + 2b(z)$.

7.2.2. ESTIMATION OF THE SINGULAR VALUE

Estimation of λ_2 : We first have

$$\begin{aligned} \lambda_2 &= \mathcal{T}_2(u_2, v_2, w_2) = \mathcal{T}_1(u_2, v_2, w_2) - \gamma \langle u_1, u_2 \rangle \mathcal{T}_1(u_1, v_2, w_2) \\ &= \mathcal{S}(u_2, v_2, w_2) + \frac{1}{\sqrt{n}} \mathcal{W}(u_2, v_2, w_2) - \gamma \langle u_1, u_2 \rangle \left(\mathcal{S}(u_1, v_2, w_2) + \frac{1}{\sqrt{n}} \mathcal{W}(u_1, v_2, w_2) \right) \end{aligned}$$

where we have

$$\frac{1}{\sqrt{n}} \mathbb{E} [\mathcal{W}(u_2, v_2, w_2)] \xrightarrow{n \rightarrow \infty} -q(\lambda_2)$$

and

$$\begin{aligned} \frac{1}{\sqrt{n}} \mathbb{E} [\mathcal{W}(u_1, v_2, w_2)] &= \frac{1}{\sqrt{n}} \sum_{ijk} \mathbb{E} [u_{1i} v_{2j} w_{2k} W_{ijk}] \\ &= \frac{1}{\sqrt{n}} \sum_{ijk} \mathbb{E} \left[\frac{\partial u_{1i}}{\partial W_{ijk}} v_{2j} w_{2k} \right] + \mathbb{E} \left[u_{1i} \frac{\partial v_{2j}}{\partial W_{ijk}} w_{2k} \right] + \mathbb{E} \left[u_{1i} v_{2j} \frac{\partial w_{2k}}{\partial W_{ijk}} \right] \end{aligned}$$

Again, we have

$$\frac{\partial u_{2i}}{\partial W_{ijk}} \simeq \frac{-1}{\sqrt{n}} v_{2j} w_{2k} Q_{ii}^{11}(\lambda_2), \quad \frac{\partial v_{2j}}{\partial W_{ijk}} \simeq \frac{-1}{\sqrt{n}} u_{2i} w_{2k} Q_{jj}^{22}(\lambda_2), \quad \frac{\partial w_{2k}}{\partial W_{ijk}} \simeq \frac{-1}{\sqrt{n}} u_{2i} v_{2j} Q_{kk}^{33}(\lambda_2)$$

Therefore

$$\begin{aligned} \frac{1}{\sqrt{n}} \mathbb{E} [\mathcal{W}(u_1, v_2, w_2)] &\simeq -\frac{1}{n} \sum_{ijk} \mathbb{E} [v_{1j} w_{1k} v_{2j} w_{2k} R_{ii}^{11}(\lambda_1)] - \frac{1}{n} \sum_{ijk} \mathbb{E} [u_{1i} u_{2i} w_{2k}^2 Q_{jj}^{22}(\lambda_2)] - \frac{1}{n} \sum_{ijk} \mathbb{E} [u_{1i} v_{2j}^2 u_{2i} Q_{kk}^{33}(\lambda_2)] \\ &\xrightarrow{n \rightarrow \infty} -\langle v_1, v_2 \rangle \langle w_1, w_2 \rangle r_1(\lambda_1) - \langle u_1, u_2 \rangle q_2(\lambda_2) - \langle u_1, u_2 \rangle q_3(\lambda_2) \\ &= -\langle v_1, v_2 \rangle \langle w_1, w_2 \rangle r_1(\lambda_1) - \langle u_1, u_2 \rangle [q_2(\lambda_2) + q_3(\lambda_2)] \end{aligned}$$

Hence, λ_2 satisfies

$$\begin{aligned} \lambda_2 + q(\lambda_2) - \gamma \langle u_1, u_2 \rangle \langle v_1, v_2 \rangle \langle w_1, w_2 \rangle r_1(\lambda_1) - \gamma \langle u_1, u_2 \rangle^2 [q_2(\lambda_2) + q_3(\lambda_2)] \\ = \mathcal{S}(u_2, v_2, w_2) - \gamma \langle u_1, u_2 \rangle \mathcal{S}(u_1, v_2, w_2) \end{aligned} \quad (39)$$

And by symmetry, from (3) and since \mathcal{T}_1 is cubic, we have

$$f_q(\lambda_2) - \frac{\gamma \kappa \eta^2}{3} r(\lambda_1) - 2\gamma \kappa^2 b(\lambda_2) = \sum_{i=1}^2 \beta_i \theta_{2i} \rho_{2i}^2 - \gamma \kappa \sum_{i=1}^2 \beta_i \rho_{1i} \rho_{2i}^2 \quad (40)$$

where we denoted $f_q(z) = z + q(z)$ and

$$\theta_{2i} = \langle u_2, x_i \rangle, \quad \rho_{2i} = \langle v_2, y_i \rangle = \langle w_2, z_i \rangle, \quad \kappa = \langle u_1, u_2 \rangle, \quad \eta = \langle v_1, v_2 \rangle = \langle w_1, w_2 \rangle$$

7.2.3. ESTIMATION OF THE ALIGNMENTS

Estimation of $\langle u_2, x_s \rangle$: From the identity in (29), we have

$$\begin{aligned} \lambda_2 \langle u_2, x_s \rangle &= \mathcal{T}_2(x_s, v_2, w_2) = \mathcal{T}_1(x_s, v_2, w_2) - \gamma \langle u_1, x_s \rangle \mathcal{T}_1(u_1, v_2, w_2) \\ &= \mathcal{S}(x_s, v_2, w_2) + \frac{1}{\sqrt{n}} \mathcal{W}(x_s, v_2, w_2) - \gamma \langle u_1, x_s \rangle \left(\mathcal{S}(u_1, v_2, w_2) + \frac{1}{\sqrt{n}} \mathcal{W}(u_1, v_2, w_2) \right) \end{aligned}$$

where

$$\frac{1}{\sqrt{n}} \mathbb{E} [\mathcal{W}(x_s, v_2, w_2)] \xrightarrow{n \rightarrow \infty} -(q(\lambda_2) - q_1(\lambda_2)) \langle x_s, u_2 \rangle$$

and $\mathbb{E} \left[\frac{1}{\sqrt{n}} \mathcal{W}(u_1, v_2, w_2) \right]$ was computed previously. We therefore have

$$\begin{aligned} [\lambda_2 + q(\lambda_2) - q_1(\lambda_2)] \langle x_s, u_2 \rangle - \gamma \langle u_1, x_s \rangle [\langle v_1, v_2 \rangle \langle w_1, w_2 \rangle r_1(\lambda_1) + \langle u_1, u_2 \rangle (q_2(\lambda_2) + q_3(\lambda_2))] \\ = \mathcal{S}(x_s, v_2, w_2) - \gamma \langle x_s, u_1 \rangle \mathcal{S}(u_1, v_2, w_2) \end{aligned} \quad (41)$$

Again by symmetry, from (3) and since \mathcal{T}_1 is cubic, we have

$$[f_q(\lambda_2) - a(\lambda_2)] \theta_{2s} - \gamma \rho_{1s} \left[\frac{\eta^2}{3} r(\lambda_1) + 2\kappa b(\lambda_2) \right] = \sum_{i=1}^2 \beta_i \langle x_s, x_i \rangle \rho_{2i}^2 - \gamma \rho_{1s} \sum_{i=1}^2 \beta_i \rho_{1i} \rho_{2i}^2 \quad \text{for } s \in [2] \quad (42)$$

Estimation of $\langle u_1, u_2 \rangle$: Again from (29), we have

$$\lambda_2 \langle u_1, u_2 \rangle = \mathcal{T}_2(u_1, v_2, w_2)$$

with $\mathcal{T}_2 = \mathcal{T}_1 - \gamma u_1 \otimes \mathcal{T}_1(u_1, \cdot, \cdot)$, therefore

$$\begin{aligned} \lambda_2 \langle u_1, u_2 \rangle &= \mathcal{T}_1(u_1, v_2, w_2) - \gamma \mathcal{T}_1(u_1, v_2, w_2) = (1 - \gamma) \mathcal{T}_1(u_1, v_2, w_2) \\ &= (1 - \gamma) \left(\mathcal{S}(u_1, v_2, w_2) + \frac{1}{\sqrt{n}} \mathcal{W}(u_1, v_2, w_2) \right) \end{aligned} \quad (43)$$

Hence, we have

$$[\lambda_2 + (1 - \gamma)(q_2(\lambda_2) + q_3(\lambda_2))] \langle u_1, u_2 \rangle = (1 - \gamma) [\mathcal{S}(u_1, v_2, w_2) - \langle v_1, v_2 \rangle \langle w_1, w_2 \rangle r_1(\lambda_1)] \quad (44)$$

Again by symmetry, from (3) and since \mathcal{T}_1 is cubic, we have

$$\boxed{[\lambda_2 + 2(1 - \gamma)b(\lambda_2)] \kappa = (1 - \gamma) \left[\sum_{i=1}^2 \beta_i \rho_{1i} \rho_{2i}^2 - \frac{\eta^2}{3} r(\lambda_1) \right]} \quad (45)$$

Estimation of $\langle v_2, y_s \rangle$: From (29), we have

$$\begin{aligned} \lambda_2 \langle v_2, y_s \rangle &= \mathcal{T}_2(u_2, y_s, w_2) = \mathcal{T}_1(u_2, y_s, w_2) - \gamma \langle u_1, u_2 \rangle \mathcal{T}_1(u_1, y_s, w_2) \\ &= \mathcal{S}(u_2, y_s, w_2) + \frac{1}{\sqrt{n}} \mathcal{W}(u_2, y_s, w_2) - \gamma \langle u_1, u_2 \rangle \left[\mathcal{S}(u_1, y_s, w_2) + \frac{1}{\sqrt{n}} \mathcal{W}(u_1, y_s, w_2) \right] \end{aligned}$$

And as previously, we have

$$\mathbb{E} \left[\frac{1}{\sqrt{n}} \mathcal{W}(u_2, y_s, w_2) \right] \xrightarrow{n \rightarrow \infty} -(q(\lambda_2) - q_2(\lambda_2)) \langle y_s, v_2 \rangle$$

And

$$\begin{aligned} \mathbb{E} \left[\frac{1}{\sqrt{n}} \mathcal{W}(u_1, y_s, w_2) \right] &= \frac{1}{\sqrt{n}} \sum_{ijk} y_{sj} \mathbb{E} \left[\frac{\partial u_{1i}}{\partial W_{ijk}} w_{2k} + u_{1i} \frac{\partial w_{2k}}{\partial W_{ijk}} \right] \\ &\simeq -\frac{1}{n} \sum_{ijk} y_{sj} \mathbb{E} [v_{1j} w_{1k} R_{ii}^{11}(\lambda_1) w_{2k} + u_{1i} u_{2i} v_{2j} Q_{kk}^{33}(\lambda_2)] \\ &\xrightarrow{n \rightarrow \infty} -\langle y_s, v_1 \rangle \langle w_1, w_2 \rangle r_1(\lambda_1) - \langle y_s, v_2 \rangle \langle u_1, u_2 \rangle q_3(\lambda_2) \end{aligned}$$

Therefore,

$$\begin{aligned} [\lambda_2 + q(\lambda_2) - q_2(\lambda_2) - \gamma \langle u_1, u_2 \rangle^2 q_3(\lambda_2)] \langle v_2, y_s \rangle &= \\ \mathcal{S}(u_2, y_s, w_2) - \gamma \langle u_1, u_2 \rangle [\mathcal{S}(u_1, y_s, w_2) - \langle v_1, y_s \rangle \langle w_1, w_2 \rangle r_1(\lambda_1)] \end{aligned} \quad (46)$$

Again by symmetry, from (3) and since \mathcal{T}_1 is cubic, we have

$$\boxed{[f_q(\lambda_2) - (1 + \gamma \kappa^2) b(\lambda_2)] \rho_{2s} = \sum_{i=1}^2 \beta_i \theta_{2i} \rho_{2i} \langle y_s, y_i \rangle - \gamma \kappa \left[\sum_{i=1}^2 \beta_i \rho_{1i} \rho_{2i} \langle y_s, y_i \rangle - \frac{\rho_{1s} \eta}{3} r(\lambda_1) \right] \quad \text{for } s \in [2]} \quad (47)$$

Estimation of $\langle v_1, v_2 \rangle$: From (29), we have

$$\begin{aligned} \lambda_2 \langle v_1, v_2 \rangle &= \mathcal{T}_2(u_2, v_1, w_2) = \mathcal{T}_1(u_2, v_1, w_2) - \gamma \langle u_1, u_2 \rangle \mathcal{T}_1(u_1, v_1, w_2) \\ &= \mathcal{S}(u_2, v_1, w_2) + \frac{1}{\sqrt{n}} \mathcal{W}(u_2, v_1, w_2) - \gamma \langle u_1, u_2 \rangle \left[\mathcal{S}(u_1, v_1, w_2) + \frac{1}{\sqrt{n}} \mathcal{W}(u_1, v_1, w_2) \right] \end{aligned}$$

Where

$$\begin{aligned}
 \mathbb{E} \left[\frac{1}{\sqrt{n}} \mathcal{W}(u_2, v_1, w_2) \right] &= \frac{1}{\sqrt{n}} \sum_{ijk} \mathbb{E}[u_{2i} v_{1j} w_{2k} W_{ijk}] \\
 &= \frac{1}{\sqrt{n}} \sum_{ijk} \mathbb{E} \left[\frac{\partial u_{2i}}{\partial W_{ijk}} v_{1j} w_{2k} + u_{2i} \frac{\partial v_{1j}}{\partial W_{ijk}} w_{2k} + u_{2i} v_{1j} \frac{\partial w_{2k}}{\partial W_{ijk}} \right] \\
 &\simeq -\frac{1}{n} \sum_{ijk} \mathbb{E} [v_{2j} w_{2k} Q_{ii}^{11}(\lambda_2) v_{1j} w_{2k} + u_{2i} u_{1i} w_{1k} R_{jj}^{22}(\lambda_1) w_{2k} + u_{2i} v_{1j} u_{2i} v_{2j} Q_{kk}^{33}(\lambda_2)] \\
 &\xrightarrow{n \rightarrow \infty} -\langle v_1, v_2 \rangle [q_1(\lambda_2) + q_3(\lambda_2)] - \langle u_1, u_2 \rangle \langle w_1, w_2 \rangle r_2(\lambda_1)
 \end{aligned}$$

And

$$\begin{aligned}
 \mathbb{E} \left[\frac{1}{\sqrt{n}} \mathcal{W}(u_1, v_1, w_2) \right] &= \frac{1}{\sqrt{n}} \sum_{ijk} \mathbb{E}[u_{1i} v_{1j} w_{2k} W_{ijk}] \\
 &= \frac{1}{\sqrt{n}} \sum_{ijk} \mathbb{E} \left[\frac{\partial u_{1i}}{\partial W_{ijk}} v_{1j} w_{2k} + u_{1i} \frac{\partial v_{1j}}{\partial W_{ijk}} w_{2k} + u_{1i} v_{1j} \frac{\partial w_{2k}}{\partial W_{ijk}} \right] \\
 &\simeq -\frac{1}{n} \sum_{ijk} \mathbb{E} [v_{1j} w_{1k} R_{ii}^{11}(\lambda_1) v_{1j} w_{2k} + u_{1i}^2 w_{1k} w_{2k} R_{jj}^{22}(\lambda_1) + u_{1i} v_{1j} u_{2i} v_{2j} Q_{kk}^{33}(\lambda_2)] \\
 &\xrightarrow{n \rightarrow \infty} -\langle w_1, w_2 \rangle [r_1(\lambda_1) + r_2(\lambda_1)] - \langle u_1, u_2 \rangle \langle v_1, v_2 \rangle q_3(\lambda_2)
 \end{aligned}$$

Hence, we have

$$\begin{aligned}
 &[\lambda_2 + q_1(\lambda_2) + q_3(\lambda_2) - \gamma \langle u_1, u_2 \rangle^2 q_3(\lambda_2)] \langle v_1, v_2 \rangle + [(1 - \gamma) r_2(\lambda_1) - r_1(\lambda_1)] \langle u_1, u_2 \rangle \langle w_1, w_2 \rangle \\
 &= \mathcal{S}(u_2, v_1, w_2) - \gamma \langle u_1, u_2 \rangle \mathcal{S}(u_1, v_1, w_2)
 \end{aligned} \tag{48}$$

Finally by symmetry, from (3) and since \mathcal{T}_1 is cubic, we have

$$\left[\lambda_2 + a(\lambda_2) + (1 - \gamma \kappa^2) b(\lambda_2) - \frac{\gamma \kappa}{3} r(\lambda_1) \right] \eta = \sum_{i=1}^2 \beta_i \theta_{2i} \rho_{1i} \rho_{2i} - \gamma \kappa \sum_{i=1}^2 \beta_i \rho_{1i}^2 \rho_{2i} \tag{49}$$

7.2.4. SYSTEM OF EQUATIONS

The second deflation step is therefore governed by the following system of equations

$$\begin{cases}
 [2b(z) + z] a(z) + \frac{1}{3} = 0 \\
 (a(z) + z - \tau b(z)) b(z) + \frac{1}{3} = 0 \\
 q(z) = a(z) + 2b(z) \\
 f_q(\lambda_2) - \frac{\gamma \kappa \eta^2}{3} r(\lambda_1) - 2\gamma \kappa^2 b(\lambda_2) = \sum_{i=1}^2 \beta_i \theta_{2i} \rho_{2i}^2 - \gamma \kappa \sum_{i=1}^2 \beta_i \rho_{1i} \rho_{2i}^2 \\
 [f_q(\lambda_2) - a(\lambda_2)] \theta_{2s} - \gamma \rho_{1s} \left[\frac{\eta^2}{3} r(\lambda_1) + 2\kappa b(\lambda_2) \right] = \sum_{i=1}^2 \beta_i \langle x_s, x_i \rangle \rho_{2i}^2 - \gamma \rho_{1s} \sum_{i=1}^2 \beta_i \rho_{1i} \rho_{2i}^2 \\
 [\lambda_2 + 2(1 - \gamma) b(\lambda_2)] \kappa = (1 - \gamma) \left[\sum_{i=1}^2 \beta_i \rho_{1i} \rho_{2i}^2 - \frac{\eta^2}{3} r(\lambda_1) \right] \\
 [f_q(\lambda_2) - (1 + \gamma \kappa^2) b(\lambda_2)] \rho_{2s} = \sum_{i=1}^2 \beta_i \theta_{2i} \rho_{2i} \langle y_s, y_i \rangle - \gamma \kappa \left[\sum_{i=1}^2 \beta_i \rho_{1i} \rho_{2i} \langle y_s, y_i \rangle - \frac{\rho_{1s} \eta}{3} r(\lambda_1) \right] \\
 [\lambda_2 + a(\lambda_2) + (1 - \gamma \kappa^2) b(\lambda_2) - \frac{2\kappa}{3} r(\lambda_1)] \eta = \sum_{i=1}^2 \beta_i \theta_{2i} \rho_{1i} \rho_{2i} - \gamma \kappa \sum_{i=1}^2 \beta_i \rho_{1i}^2 \rho_{2i}
 \end{cases} \tag{50}$$

with $f_q(z) = z + q(z)$ and $\tau = \gamma \kappa^2 - 1 + \kappa(\gamma - 1)$. In the case $\gamma = 1$, we have $\kappa = 0$ from (43) and therefore the system above reduces to the following system, since $a(z) = b(z) = \frac{r(z)}{3}$ and $q(z) = r(z)$.

$$\begin{cases}
 f_r(\lambda_2) = \sum_{i=1}^2 \beta_i \theta_{2i} \rho_{2i}^2 \\
 h_r(\lambda_2) \theta_{2s} - \frac{\eta^2}{3} r(\lambda_1) \rho_{1s} = \sum_{i=1}^2 \beta_i \langle x_s, x_i \rangle \rho_{2i}^2 - \rho_{1s} \sum_{i=1}^2 \beta_i \rho_{1i} \rho_{2i}^2 \\
 h_r(\lambda_2) \rho_{2s} = \sum_{i=1}^2 \beta_i \theta_{2i} \rho_{2i} \langle y_s, y_i \rangle \\
 [\lambda_2 + \frac{2}{3} r(\lambda_2)] \eta = \sum_{i=1}^2 \beta_i \theta_{2i} \rho_{1i} \rho_{2i}
 \end{cases} \tag{51}$$

8. Algorithms

Algorithm 1 below, implements the fixed point equation in Definition 3.4 which allows the computation of the Stieltjes transform at the second deflation step.

Algorithm 1 Stieltjes Transform by Fixed Point

Input: $z \in \mathbb{C} \setminus \text{supp}(\nu)$ and τ .
 - Initialize a and b .
repeat
 - Update $a \leftarrow \frac{-1}{3(2b+z)}$.
 - Update $b \leftarrow \frac{-1}{3(a+z-\tau b)}$.
until convergence.
Output: a, b and Stieltjes transform $q = a + 2b$.

Algorithm 2 implements our RTT-improved tensor deflation procedure which is described in more details in Section 3.3.

Algorithm 2 RTT-Improved Tensor Deflation Algorithm

Input: Tensor $\mathcal{T} \in \mathbb{R}^{p \times p \times p}$ and step size $\epsilon \in [0, 1]$.
 # Perform orthogonalized deflation:
 1- Compute $\hat{\lambda}_1 \hat{u}_1 \otimes \hat{v}_1 \otimes \hat{w}_1$ as best rank-one approximation of \mathcal{T} .
 2- Compute $\hat{\lambda}_2 \hat{u}_2 \otimes \hat{v}_2 \otimes \hat{w}_2$ as best rank-one approximation of $\mathcal{T} \times_1 (\mathbf{I}_p - \gamma \hat{u}_1 \hat{u}_1^\top)$ for $\gamma = 1$.
 # Estimate underlying model parameters:
 3- Compute $\hat{\eta} \leftarrow |\langle \hat{v}_1, \hat{v}_2 \rangle|$.
 4- Estimate $\hat{\beta} = (\hat{\beta}_1, \hat{\beta}_2, \hat{\alpha})$ and $\hat{\rho} = (\hat{\rho}_{1i}, \hat{\rho}_{2i}, \hat{\theta}_{2i} \mid i \in [2])$ by fixing $\hat{\lambda} = (\hat{\lambda}_1, \hat{\lambda}_2, \hat{\eta})$ and solving $\psi(\hat{\beta}, \hat{\lambda}, \hat{\rho}) = 0$ in $\hat{\beta}$ and $\hat{\rho}$ with ψ defined in (16).
 # Estimate optimal γ :
 5- Initialize $\gamma = 1$ and $\hat{\kappa} = 10^{-5}$.
 6- Initialize two empty lists L_γ and L_ρ .
repeat
 7- Set $x_0 \leftarrow (\hat{\lambda}_2, \hat{\kappa}, \hat{\eta}, \hat{\theta}_{2i}, \hat{\rho}_{2i} \mid i \in [2])$.
 8- Estimate $(\hat{\lambda}_2, \hat{\kappa}, \hat{\eta}, \hat{\theta}_{2i}, \hat{\rho}_{2i} \mid i \in [2])$ by solving the system in (14) initialized with x_0 and for $(\beta_1, \beta_2, \alpha) = (\hat{\beta}_1, \hat{\beta}_2, \hat{\alpha})$ and γ .
 9- Append L_γ with γ .
 10- Append L_ρ with $\max\{\hat{\rho}_{21}, \hat{\rho}_{22}\}$.
 11- Update $\gamma \leftarrow \gamma - \epsilon$.
until The maximum is reached in L_ρ .
 12- Set optimal γ as $\gamma^* \leftarrow L_\gamma[\arg \max(L_\rho)]$.
 # Perform orthogonalized deflation with γ^* :
 13- Compute $\hat{\lambda}_2 \hat{u}_2 \otimes \hat{v}_2^* \otimes \hat{w}_2^*$ as best rank-one approximation of $\mathcal{T} \times_1 (\mathbf{I}_p - \gamma^* \hat{u}_1 \hat{u}_1^\top)$.
 14- Compute $\hat{\lambda}_2 \hat{u}_2^* \otimes \hat{v}_2 \otimes \hat{w}_2^*$ as best rank-one approximation of $\mathcal{T} \times_2 (\mathbf{I}_p - \gamma^* \hat{v}_1 \hat{v}_1^\top)$.
 # Re-estimate the first component by simple deflation:
 15- Compute $\hat{\lambda}_1 \hat{u}_1^* \otimes \hat{v}_1^* \otimes \hat{w}_1^*$ as best rank-one approximation of $\mathcal{T} - \min\{\hat{\beta}_1, \hat{\beta}_2\} \hat{u}_2^* \otimes \hat{v}_2^* \otimes \hat{w}_2^*$.
Output: Estimates of the signal components $(\max\{\hat{\beta}_1, \hat{\beta}_2\}, \hat{u}_1^*, \hat{v}_1^*, \hat{w}_1^*), (\min\{\hat{\beta}_1, \hat{\beta}_2\}, \hat{u}_2^*, \hat{v}_2^*, \hat{w}_2^*)$.
